SRJMET

Scientific Research Journal for Metal Engineering and Technologies
Volume No.01 Issue No. 01, PP 63 - 70

ISSN:399-2017
01. Jan.2018

The Effect of Arc Pulsation in DCGTA Welding on the Microstructure and Hardness of the Weld Metal of 304 L Stainless Steel

Fouad B. Abudaia[a], Moammar Elhadi Attaya[a]and **Azaldin Alhaj Kozam[b]**

fabudaia@yahoo.com

a) University of Tripoli, Department of materials and Metallurgical Eng.

b) Advanced Occupational Center for Welding Technologies

Abstract

The effect of pulsating current compared with continuous non-pulsating current in GTA welding on the weld metal microstructure of 304 L austenitic stainless steel was investigated. In this study, two joints of 2 mm thick were prepared for welding with non-pulsating Direct Current (DC) and a 10 Hz DC pulsating current Hardness measurements and metallographic examinations were carried out to assess the effect of the pulsating current over the non-pulsating current. The results showed that using pulsating current produced smaller weld pool with relatively finer dendritic structure and higher hardness in the solidified weld metal. The microstructure of the non-pulsating current showed that the solidification mode is ferrite austenite mode (FA mode) where the liquid metal solidifies as ferrite dendrites which later transform to austenite leaving the core of dendrites as a skeleton of ferrite. However, the joints welded with the pulsating current showed that the transformation mode is partially changed to austenite mode (A mode) in some areas of the weld metal. The change in the solidification mode is thought to be due to the increased cooling rate because of the decreased heat input of the pulsating current compared with the non-pulsating current.

Key words: Gas Tungsten Arc Welding, Arc Pulsation, solidification mode.

SRJMET

Scientific Research Journal for Metal Engineering and Technologies
Volume No.01 Issue No. 01, PP 63 - 70

ISSN:399-2017
01. Jan.2018

1. Introduction.

In fusion welding joining of metals is achieved by providing sufficient heat energy to melt both ends of the joint in one weld pool to solidify as one part. A successful welded joint should contain no defects in the weld metal and the Heat Affected Zone (HAZ)or at least the severity of these defects is within the accepted limits. As a rule of thumb excessive provided heat energy known as the heat input would increase the size of the weld pool and the HAZand causes more distortion to the welded joint. Even when there is no defects or discontinuities in the weld metal or the HAZ softening could took place in some metals and alloys due to grain growth or other metallurgical changes such as second phase particle coarsening or over aging. These changes become more pronounced with increasing the heat input. Thus refining the solidified structure will avoidor limits softening or even increases the hardness of the weld metal. One approach to achieve this goal is by use of pulsating current instead of continuous (or non-pulsating current) in DC welding. The high level of the peak current is selectedto give adequate penetration while the bottom current is set at a levelsufficient to maintain a stable arc. [1]. So the aim of this work is to investigate the effect of using pulsating current compared with non-pulsating current on the structure and hardness of the weld metal of 304 L austenitic stainless steel in GTA welding

2. Experimental Procedure

2.1 Material

The chemical composition of the 304L stainless steel is as given in table 1.The composition was obtained using spectrometer analysis

Sheets with dimensions 100 x15x2 mm were cut and square but joints were prepared for welding. The as received sheets were solution treated by heating to 900 ºC for half an hour then quenched in water.

Table 1: the chemical composition of the welded steel.

Element	C	Si	Mn	Cr	Ni	P	S	Fe
wt%	0.03	0.5	1.5	18.0	9.0	0.04	0.03	balance

2.2 Welding

Joints were welded using GTA welding without gap using filler rods SFA 5.1 ER 308L with 1.6 mm diameterand 70 Ampere DC current electrode negative and welding velocity 60 mm/min. Argon gas was used as a shielding gas at a rate of 8 liters/min and purged below the joint at rate of 4 liter/min. For joints welded using pulsating current, the wave cycle with 10 Hz was used with 50 % pulse on time as shown schematically in figure 1 with 35 Ampere base currentand peak current of 70 Ampere.

2.3 Metallographic Examination and Micro-hardness test

Samples for metallographic examination of the welded joints were cut to inspect the cross sectional sides of the welded join as shown in figure 2. Specimens were prepared by grinding, polishing and then etched using Glyceregia reagent. Optical microscope was used to examine the microstructure and microhardness tester type Microbul-1000 DN to measure the hardness on polished un-etched samples. Tenmicrohardness readings were taken inside the weld metal and covered all the cross section of the weld metal in both samples.Width of the weld metal (solidified weld pool) was measured with the aid of the stage micrometer on the same microhardness tester by moving the sample transversely across the stage from one end of the weld metal till the other end.

SRJMET

Scientific Research Journal for Metal Engineering and Technologies
Volume No.01 Issue No. 01, PP 63 - 70

ISSN:399-2017
01. Jan.2018

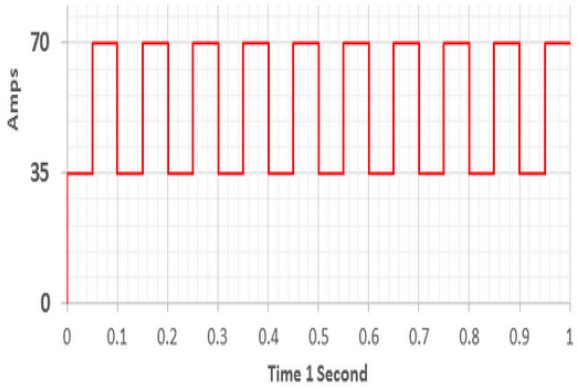

Figure 1: the welding current cycle of 10 Hz

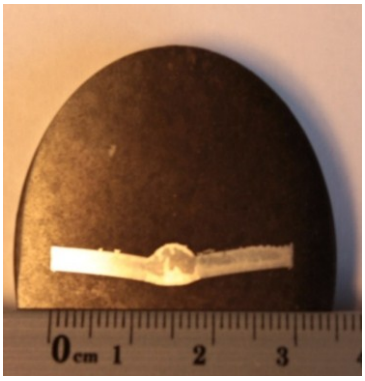

Figure 2: shows cross section of a welded joint.

3. Results

Microstructures of non-pulsating and the 10 Hz DC pulsed currentwelded joints are shown in figure 3 a & b respectively at magnification of 500 x

The results of weld metal microhardness and widths of the weld metal zones are shown in table 2where the minimum and maximum microhardness reading are indicated.

Schematic drawing of the weld pool size (or weld metal) is also shown in figure 4 for illustration.

Table 2: results of microhardness and widths ofweldmetal for pulsating and non-pulsating currents

Method of GTA welding	MicrohardnessHv	Weld metal width (mm)
Continuous –non-pulsating	177-200	7.3
10 Hz pulsating current	189-215	5.7

SRJMET

Scientific Research Journal for Metal Engineering and Technologies
Volume No.01 Issue No. 01, PP 63 - 70

ISSN:399-2017
01. Jan.2018

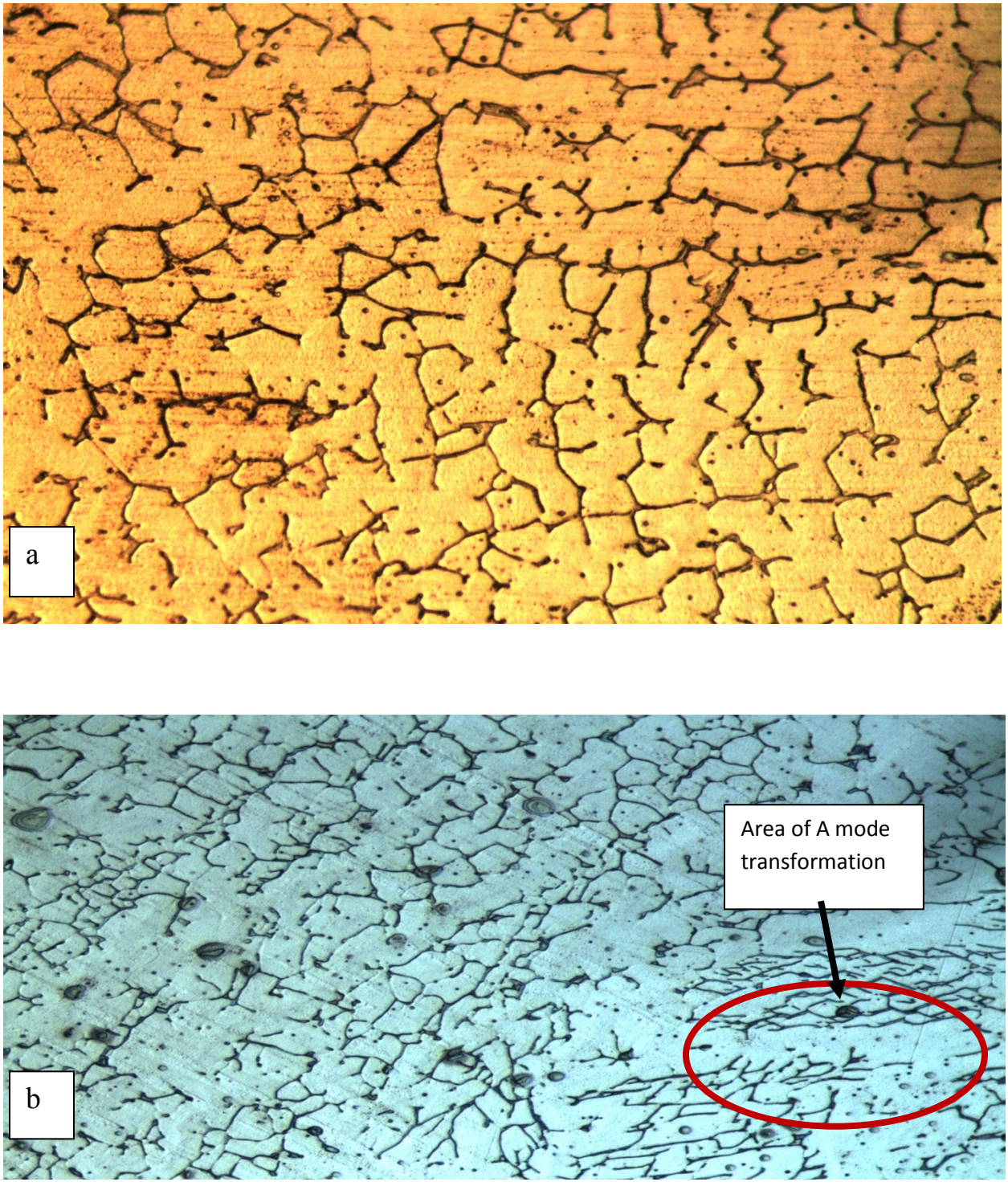

Figure 3: a) shows the microstructures of welded joint using continuous non-pulsating DC and b) the microstructure for welded joint using 10 Hz pulsed current

SRJMET

Scientific Research Journal for Metal Engineering and Technologies
Volume No.01 Issue No. 01, PP 63 - 70

ISSN:399-2017
01. Jan.2018

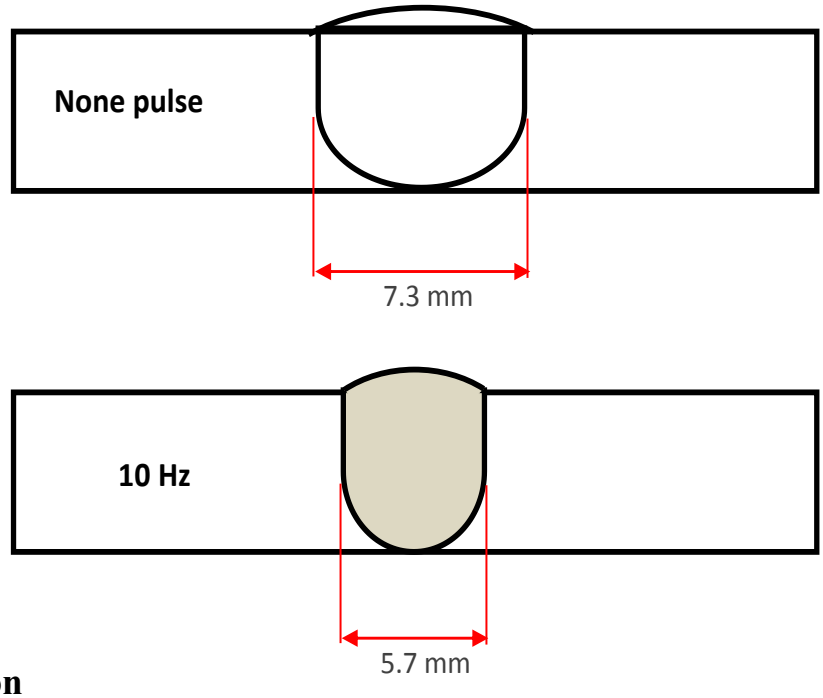

4. Discussion

From the chemical composition of this steel, the Cr equivalent=18.75 and the Nickel equivalent =10.75 and the Creq.to Ni eq. ratio is about 1.85. When this ratio is between 1.5 and 1.9 the microstructure is expected to consist of continuous austenite phase with skeleton of the primarily formed ferrite dendrites which appear as dark branches in the microstructure which is atypical structure for FA mode [2]. Even if the dilution from the filler rod 308 L is taken in to consideration the solidification mode would not be changed because the Creq.to Ni eq. ratio of the filler rod SFA 5.1 ER 308L is higher than 1.6.

The microstructure of joint welded using 10 Hz pulsating current showed that the transformation mode is mixed. In addition to the FA mode which prevails in the microstructure some parts as in the encircled area were transformed in A mode where the transformation is starts and finishes as austenite phase [3]. Another noticeable effect of the pulsating current is the decrease in the dendrites sizes in the microstructure of joint welded by pulsed current compared with the non-pulsating current as can seen by comparing the two micrographs.

The finer structure produced by the pulsating current caused an increase in the hardness of the weld metal as shown in table 2. The enhance of mechanical properties of welded metal welded using pulsating current wasreported by Rani and Marpu, they found increase in tensile and yield strength of joints welded by pulsating current with 7 Hz compared with joints welded by non-pulsating current in GTA welding [4] The weld pool size itself become smaller as shown in the table 2 and explained by the schematic drawing in figure 3.

The change in microstructure caused by the pulsating current is related to the increased cooling rate due to the lowered heat input in the welding process. In this welding process the current at the bottom of the wave was 50% of the upper value, this mean that the heat input received by the joint welded by pulsating current is reduced by 25 % compared with the non-pulsating current. The lower heat input reduces the weld pool size. The faster cooling rate produces finer structure with increased hardness. These changes are beneficial which gives higher strength to the welded joint and also finer structure is more resistant to crack propagation.

The other effect observed in this work is the partial change in the solidification mode from complete FA mode to FA mode with some A mode. This change will reduce the ferrite content of the welded joint of the austenitic stainless steel. In this steel and according to the calculated chromium equivalent and Nickel equivalent and according to Scheaffler diagram the ferrite content is in the range 5 to 10 % and for the filler rod is about 10.5 % according to DeLong diagram due to Nitrogen content of 0.05 in the filler rod. The ferrite content in the microstructure of pulsed current welded sample would be less than the un-pulsed welded sample due the partial change in the solidificationmode but thisdecrease in the ferrite content due to arc pulsation is expected to be minor because the prevailing solidification mode is still FA mode and the arc pulsation causes only partial change in the solidification mode Thus by assuring that the ferrite content did not decrease below about 5 % then the reduction in ferrite content

due to arc pulsation will not harm the ability of the welded 304L stainless steel to resist hot crack.

5. Conclusions

1. Using of pulsating current is beneficial in refining the microstructure. Structure refining will increase the hardness and strength of the welded joint and increases the resistance of the structure to cracking.
2. The transformation mode in 304 L SS is usually FA mode. Arc pulsation parameters as used in this study had induced limited A mode transformation but
3. the effect on the ferrite content in the weld metal is expected to be minor.

References

1. T.Senthil et al. 2007. J. Mater. Sci. Technol., Vol.23 No.2.
2. J.F. Lancaster.1984. Metallurgy of Welding 5th ed. CHAPMAN & HALL.
3. Sindo Kou.1987Welding Metallurgy. John Wiley & Sons Wiley.
4. Indira Rani and R N Marpu. 2012. The International Journal of Engineering and Science (IJES) Volume 1, Issue 1,Pages 01-05

SRJMET

Scientific Research Journal for Metal Engineering and Technologies
Volume No.01 Issue No. 01, PP 71 - 86

ISSN:399-2017
01. Jan.2018

Influence of Decarburization on the Microstructure, Hardness, Fatigue and Impact Properties of D3 Tool Steel

Abdullatif Kamshushi[a] and Mohamed Mokharm[b].

[a]**m.mokharm@hvcc.ly,** [b]**kamshushi@gmail.com**

High Vocational Centre of Casting (HVCC), Tripoli, Libya

Abstract

AISI D3 (X210Cr12) steel is a high carbon high chromium, oil hardening tool steel that is widely used in manufacturing blanking, stamping and cold forming dies and punches as well as many other cold working tools. To achieve utmost mechanical properties, the steel is subjected to hardening and tempering heat treatment. Hardening consists of austenitization at 950°C for a certain periodfollowed by quenching oil and then temperingat temperatures between 200 and 550°C for from one to two hours. When hardening is donein air atmosphere furnaces, carbon atoms at surface react with oxygen and are removed in form of gases.The carbon removal process is known as decarburization and considered detrimental to mechanical properties. This investigation examined the effect of decarburization on the microstructure, hardness, fatigue strength and impact energy of D3 tool steel. Two groups of specimens were soaked at austenitising temperature of 950ºC, the first group for one hour while the second for three hours. Following austenitization, specimens were quenched in oil and then tempered at 450°C for one hour. Microhardness profiles and microstructure examination practices were used to measure and characterize the depth of decarburized layer. A rotating bending fatigue testing machine was used to determine the fatigue strength while Charpy impact testing

machine has been used to determine the impact energy of unnotched specimens. Results obtained showed that, extending austenitising time, increases the depth of the decarburized layer and as a result, fatigue strength and surface hardness have been reduced. On the other hand, it was found that the absorbed impact energy has slightly increased with extending austenitizing time.

Key Words: Decarburization, microstructure, hardness, fatigue strength, impact energy,

1. Introduction

AISI D3 tool steel is widely used in manufacturing machine parts, dies and mouldsas well as in automotive industry. In order to extend the service life of the engineering components made of this steel, they are typically subjected to hardening and tempering heat treatment. During hardening in air atmosphere furnaces, decarburization takes place leaving behind a surface that is poor in carbon. It occurs when carbon atoms at the steel surface react with furnace atmosphere and are removed in form of gases. Carbon atoms from layers below the surface are then diffuse towards the surface to continue thedecarburization process and establishing the maximum depth of decarburization. In fact, decarburization isa serious problem as it makes surface properties inferior than that of the core. It is well known that the hardness obtained from hardening heat treatment is greatly influenced by the available carbon content in steel during quenching [1]. Decarburization results in reduction in the carbon content at the surface and consequently altering the surface mechanical properties of the steel [2]. Properties include hardness, wear resistance and fatigue strength will be reduced which makes failures during service become easier to occur.

The aim of the current investigation is to evaluate the effect of decarburization on the microstructure, surface hardness, fatigue strength and impact energy of

D3 tool steel. Different parts made of the D3 tool steel are usually held at theaustenitizing temperature for different periods depending on the size of the part.As size increases, austenitising time is more extended and accordingly a deeper decarburized layer is obtained causing the steel to be weaker. In order to investigate the influence of the decarburized layer on the pre-mentioned properties, several specimens have been austenitized for one hour and three hours at 950°Cand then immediately quenched in oil to room temperature Following hardening all specimens were tempered at 450°C for one hour.

2. Experimental Work.

TheD3 tool steel employed in the present study was received in annealing conditions having a hardness value of 23HRC. A spark emission spectrometer (model Oxford-foundry master pro) was used to determine its chemical composition and result obtained is tabulated in table 1.

Table 1: chemical composition of the investigated tool steel (wt%).

C %	Cr %	Si %	Mn %	V %	W %	P(max) %	S (max) %	Fe %
2.23	12.1	0.373	0.21	0.023	0.12	0.013	0.0073	Rem.

2.1 Metallographic Examinations

Samplesfor metallographic examination were ground using silicon carbide wet emery papers of increasing fineness namely 180, 220, 400, 600, 800 and 1200 grid and then polished using diamond pastes of 1 and 0.25 microns. The polished samples were etched in 3%Nital solution and then inspected using an optical microscope with a magnification of up to X1000 and equipped with a digital camera.

2.2 Micro hardness Measurements

Microhardness measurements were taken on samples of 10mm diameter and 20mm height that were previously austenitized for one and three hours. Following heat treatment, samples were carefully and slowly cut in the middle and then ground, polished in the standard way and etched in 3% Nital solution. Vickers micro hardness measurements were taken along a line extends from the surface towards the core of the specimens using a load of 200g,dwelling time of 10 seconds and intervals of 50 microns on a micro hardness testing machine model Micro bul 1000-DN Digital.

Microhardness profiles were plotted using hardness values that are the average of three measurements taken at the same distance from the surface as shown in figure 1. These profiles were used to measure the depth of the decarburized layer.

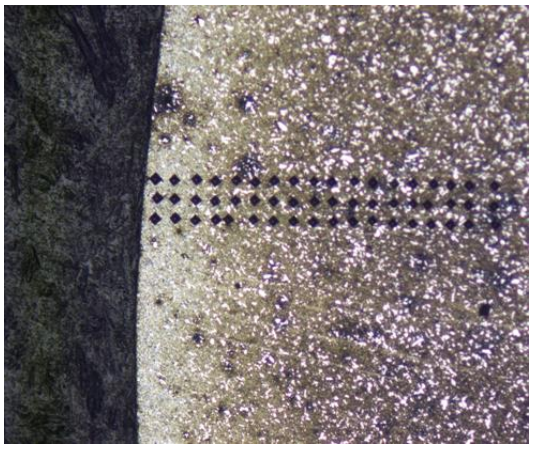

Figure 1: micro hardness measurements for specimen austenitized for one hour (100X).

2.3 Fatigue Testing

Fatigue specimens austenitized for one and three hours were used to study the effect of the depth of the decarburized layer on fatigue strength. The specimens

were machined from one bar, according to the dimensions seen in Figure (2). Each specimen was polished with emery paper to surface average roughness of R_a =0.36µm in the useful region which had a diameter of 8.0mm.Following heat treatment, specimen were slightly re-polished with 1000 grade emery paper until a mirror polish condition was achieved.

Fatigue tests were carried out at room temperature on a rotating bending fatigue machine, type Zwick/Roell, model UBM 200, shown in Figure (3).The speed kept constant at 4000RPM.

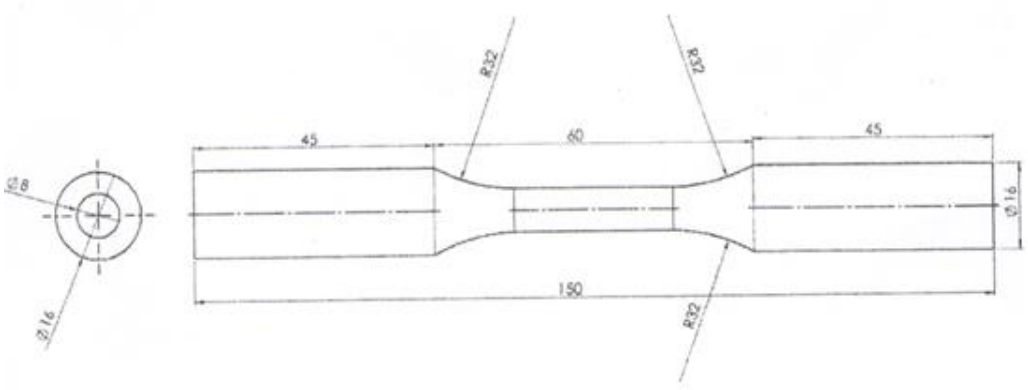

Figure 2: Dimensions of fatigue specimens.

Figure 3: Photo of the rotating bending fatigue machine, type Zwick / Roll, model UBM 200 utilized in the fatigue testing.

The specimen bending load was applied by a load arm existing in the machine. The applied stress varied from 650 to250 MPa. The true applied bending stresses (tension/compression) on the surface of fatigue specimen were calculated byequation (1), stated in the operating manual of the utilized machine.

$$\delta = \frac{M_B}{W} = \frac{G*9.81*1000*32}{d^3*\pi} = \frac{N}{mm^2} \quad \text{----------(1)}$$

where:

δ= Bending stress (tension / compression)

M_B = Bending moment = G * 9.81 * Load arm (Nm)

W = Resistance moment = $d^3 * \pi$ / 32 (mm^2)

G = Loading weight (kg)

Fatigue tests were initiated for high applied load until the specimen breaks. This high load was gradually reduced for the following specimens till failure. At each load two specimens were tested for each austenitising condition however, when it was necessary, three specimens were used. The average values were used to draw the S-N curves in order to compare the effect of the depth of the decarburized layer on fatiguestrength which was defined as the valueof stress at 10^7 cycles.

2.4 Impact Testing

Impact energy refers to the total amount of energy absorbed by a given specimen undergoing fracture when it is tested under a high strain rate or rapid loading condition. The Charpy test is the most common laboratory procedure used to measure impact energy in which a notched specimen is used. In the current study, the value of impact energy obtained in the case of a notched

specimen was in fact much lower than that obtained with an unnotched one. This variation implies that, the absorbed impact energy is dependent on the notch geometry rather than the microstructure. Thus, in order to increase the accuracy of the measurement of impact energy values, as well as to emphasize the influence of the depth of the decarburized layer, un-notched specimens were employed. The dimensions of the un-notched Charpy impact specimen used are shown in figure 4.

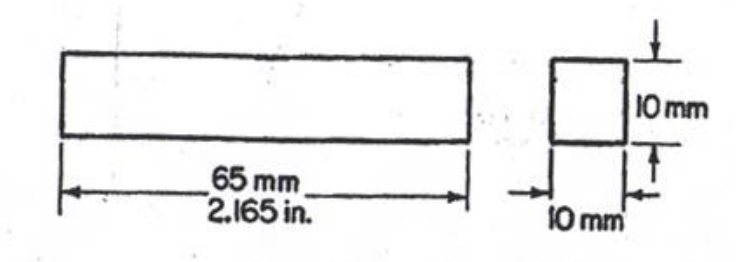

Figure 4: Dimensions of the un- notched impact samples as stated by ASTM E 23.

The absorbed impact energy of specimens austenitized for one and three hours were measured at room temperature using a pendulums impact tester, type Zwick/Roell, with 450J capacity hammer and a striking velocity of about 5.23 m per second. To determine the absorbed impact energy in each austenitising conditions three samples were used and the average values were reported.

3. Results and Discussion.

3.1 Microhardness & Microstructure.

Micro-hardness profiles are frequently used to estimate carbon content in the steel matrix as well as to measure and characterize the undesired heat treatment side effect of decarburization [3]. Figure 5 shows themicro-hardness profiles for specimens austenitized for one and three hours.

SRJMET

Scientific Research Journal for Metal Engineering and Technologies
Volume No.01 Issue No. 01, PP 71 - 86

ISSN:399-2017
01. Jan.2018

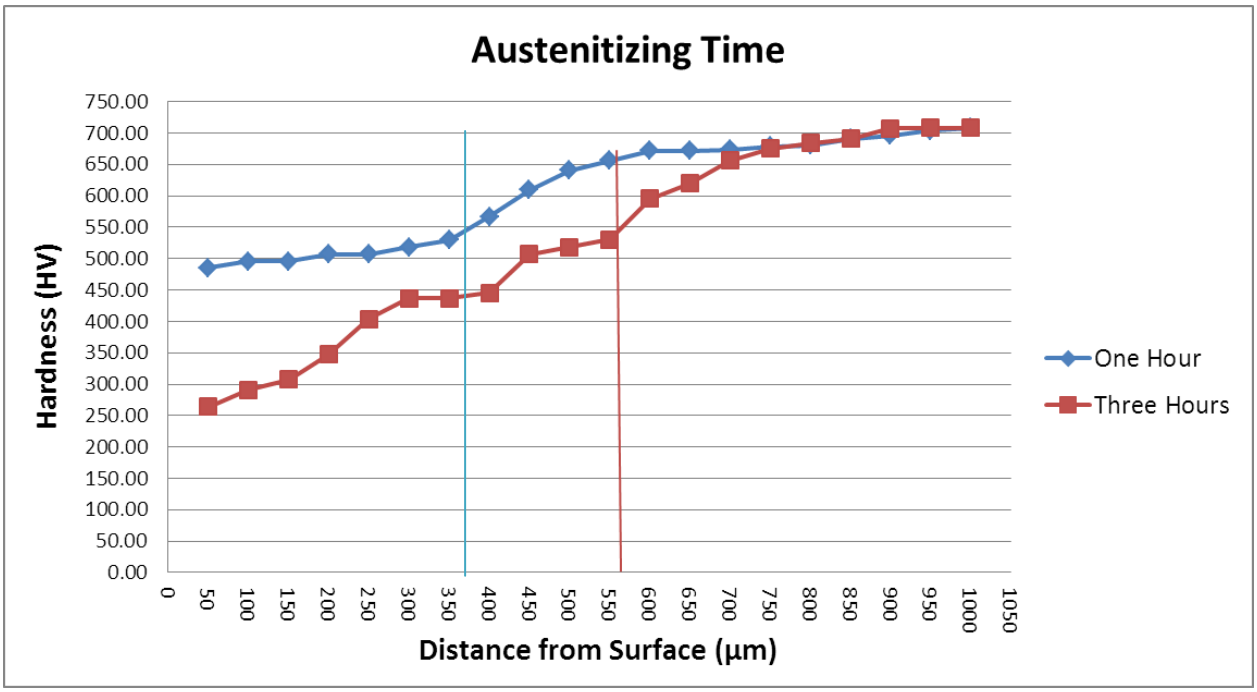

Figure 5: Micro hardness profiles for specimens austenitised for 0ne and three hours.

It can be seen from figure 5 that in both cases the hardness increases gradually from surface towards the core of the specimens and as austenitizing time is extended from one to three hours, the decarburized layer becomes deeper. The core hardness is similar in both cases namely 708 HV (59 HRC). For the purpose of this study, the depth of the decarburized layer is defined as the distance from the surface that has hardness less than 550HV (50 HRC). This makes the depth of the decarburized layer is approximately equal to 380 µm and 570 µm in specimens soaked for one and three hours respectively

The reduction in hardness of the decarburized layer is due to lowering its carbon content during austenitization. It is well known that, austenite saturated with carbon transforms to hard martensite when quenched from austenitizing temperature. On the other hand, low carbon austenite if cooled fast enough would transform to low hardness martensite which decomposesto ferrite and carbides during tempering.

SRJMET

Scientific Research Journal for Metal Engineering and Technologies
Volume No.01 Issue No. 01, PP 71 - 86

ISSN:399-2017
01. Jan.2018

Figures (6a) and (6b) show the depth of decarburized layer for specimens austenitized for one hour and three hours respectively.It can be noted that there is a great reduction in the volume fraction of primary carbides at the surface and layers beneath

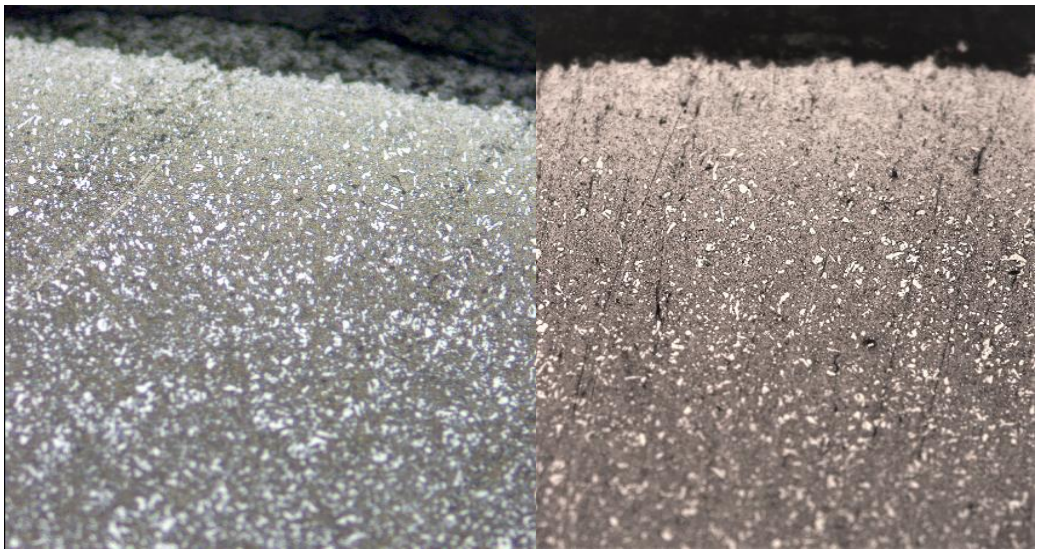

(a) (b)

Figure 6a & 6b: Depth of decarburized layer for specimens austenitised for one and three hours (200X).

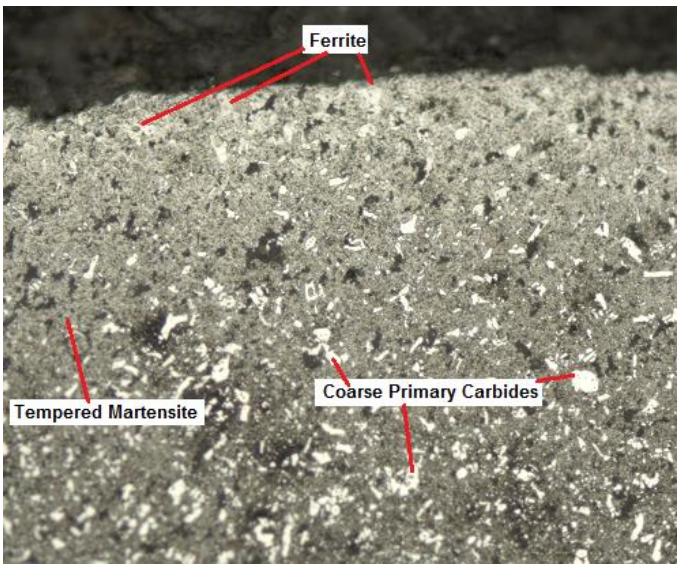

Figure 7: Microstructure of specimen austenitized for one hour (400X).

Figure 7 shows the presence of white etched areas close to the surface which have a different contrast in comparison to carbides. These areas are most likely to beferrite. The presence of the later phase and the increase in its volume fraction with extending austenitising time is thought to be the prime reason for the reduction in hardness of the decarburized layer.

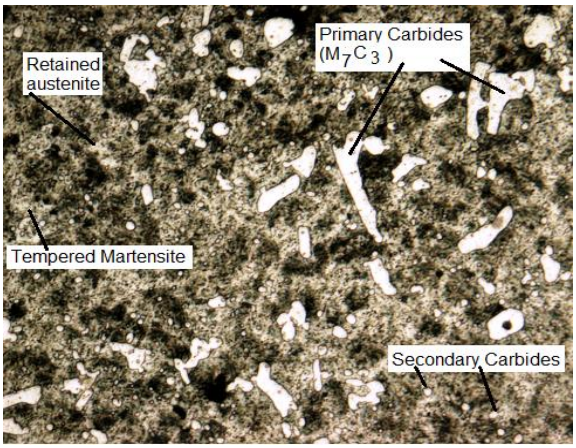

Figure 8: Microstructure of hardened D3 tool steel (1000X).

Figure 8 shows that the core microstructure of the hardened steelconsists of primary coarse carbides impeded in a tempered martensitic matrix. The isothermal section of high carbon high chromium steels shown in Figure 9 demonstrates the structures prevailing at the austenitizing temperature 1000°C [4]. It can be seen that at this temperature which is close to the utilized temperature in this study, the only type of carbides present after austenitizing at1000°C is the$(CrF_e)_7C_3$ type. . Several researches claimed that, the reduction in the volume fraction of carbides is responsible for the reduction of wear resistance of the steel [5-7].

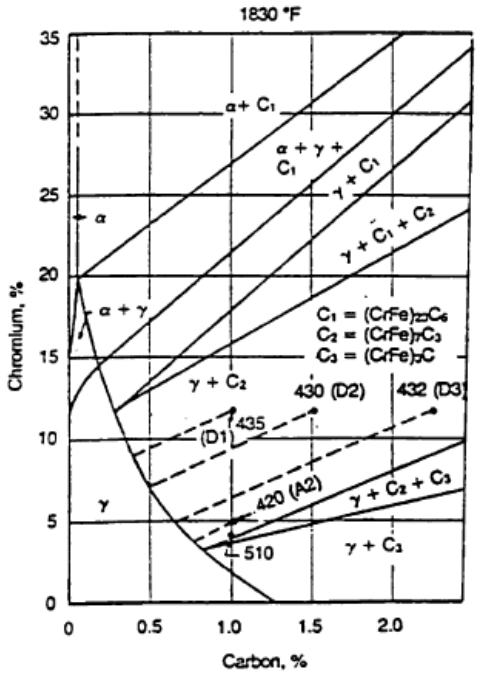

Figure (8): Isothermal section of iron-chromium-carbon system at 1000°C.

3.2 Fatigue strength

The fatigue strengthvalues for specimens austenitized for one and three hours were obtained directly from the plotted S-N curves in figure 10. Fatigue strength is the value of stress at failure for 10^7cycles.

SRJMET

Scientific Research Journal for Metal Engineering and Technologies
Volume No.01 Issue No. 01, PP 71 - 86

ISSN:399-2017
01. Jan.2018

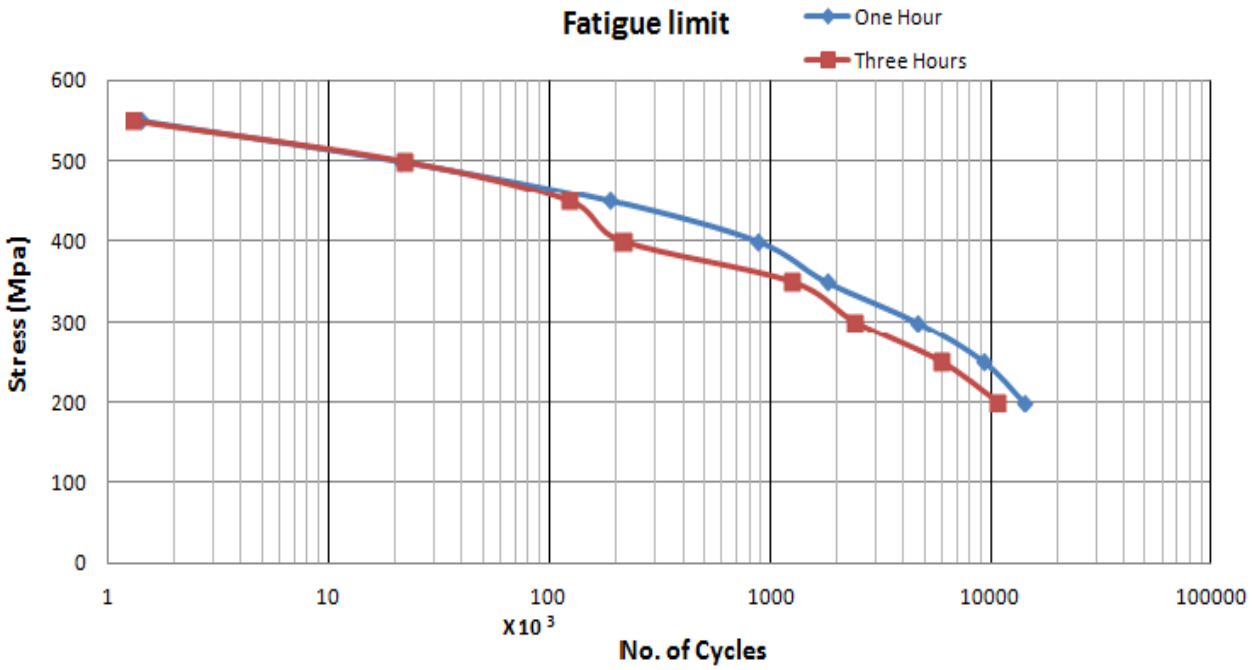

Figure (10): Stress versus number of cycles (N) curves for rotating bending fatigue test.

Table (2): Fatigue strength values obtained from the S-N

Specimen Condition	Fatigue Limit Stress (MPa)
One Hour Austenitizing Time	260
Three Hours Austenitizing Time	200

Table 2, suggests a reduction of 23% of the fatigue strength resulted from extending the austeitizing time from one to three hours.This can be referred to the increase in the depth of the decarburized layer took place. It can be claimed that, decarburization has led to formation of a soft surface has with low tensile strength and in turn low fatigue strength, consequently, crack nucleation becomes easier.

Other reason for the reduction in the fatigue strength can be attributed to the formation of residual tensile stresses on the surface. During quenching from the

austenitization temperature, the metastable austenite starts to transform to martensite at a temperature known as (Ms) temperature which is inversely related to the austenite carbon content. In other words, the reduction in carbon content raises the martensite transformation temperature (Ms). Thus, during quenching, martensitic transformation starts at the outermost surface layers due to the low carbon content. As the transformation goes deeper into the softer austenite towards the core, the increase in volume associated with this transformation, is restricted by the martensite already created in the outer regions of the part adjacent to the surface. This creates internal stresses which puts the surface in tension. In fact, the development of tensile stress on the surface lowers fatigue strength of the steel.

Furthermore, if enough martensite is formed to create internal stress greater than the ultimate tensile strength of the steel, a crack may be initiated at the surface. It is well known that fatigue properties are strongly affected by the surface conditions of the part, this includes surface roughness and surface imperfections. In this manner, decarburization can be considered as a surface defect that results in a softer surface unsuitable for any application involving wear or fatigue [9].

3.3 ImpactEnergy

Results of the un-notched Charpy Impact testing are shown in table (3). As it can be seen from this table, extending austenitizing time from one to three hours resulted in slight increase in the absorbed impact energy.

Table 3: Absorbed impact energy for specimens austenitized for one and three hours

Specimen Condition	Absorbed Impact Energy (J)
One Hour Austenitizing Time	42
Three Hours Austenitizing Time	46

Again this can be attributed to the increase in the depth of the decarburized layer resulted from extending austenitizing time. It has been shown in previous sections that decarburization lowered the hardness due to carbon loss from the steel matrix. It can also be argued that decarburization permits plastic deformation at surface,most properly due to the decrease in the volume fraction of the hard carbides and increasing the volume fraction of the soft ferrite . The reduction in the volume fraction of the most hard $(CrFe)_7C_3$-type carbides in high carbon high chromium cold work tool steelsfollowing austenitization at1150°C for 30 minutes from 9.52% to 4.80% has been reported other investigators [10]. Decarburization has slightly improved the impact energy of the steel, however, it adversely affected the fatigue strength, thus improving impact toughness by decarburization is rarely advisable.

4. Conclusions

In this study, different D3 tool steel specimens were subjected to hardening and tempering heat treatment in which specimens austenitised at 950°C. Some specimens were austenitized for one hour whilst others for three hours in an air atmosphere heat treatment furnace. Following austenitization, specimens were quenched in oil and then tempered at 450°C for one hour. In both heat treatment conditions decarburization took place at surface and sub-surface regions

however, the depth of the decarburized layer was thicker and deeper in specimens austenitised for three hours.

Decarburization has slightly improved the impact toughness however, it has a detrimental effect on other mechanical properties such as surface hardness and fatigue strength and as consequence it must be avoided. In fact, decarburization reduces the tensile strength and wear resistance of the steel as both properties are dependenton hardness.

It is highly recommended to use controlled atmosphere furnaces in hardening the high carbon steel alloys specially when it is necessary to soak parts at high temperatures for long times otherwise, removing the decarburized layer by grinding is highly recommended.

References

[1] Zhang C, Chen R, Luo F, Du C, Shi W. Effect of heat treatment process on microstructure and properties of H13 steel. JinshuRechuli/Heat treat Metals 2012, 37:119-21.

[2] M. Nomura, H. Morimoto and M. Toyama: ISIJ Int., 2000, 40, 619-623.

[3] M. Ramezani, T. Pasang, Z. Chan, T. Neitzert, D. Au. Evaluation of carbon diffusion in heat treatment of H13 steel under different atmospheric conditions. J Mat. Res. Technol. 215; 4(2) 114-125

[4] Hamaker, J. C., Jr, Die steel useful for ultra high strength structural requirements, Metal Progress (Dec 1956), P93.

[5] G. Kocher, K. Chopra, S. Kumar. Investigation on surface integrity of AISI D3 tool steel After EDM. International Journal of Technology and Advanced Engineering, Volume 2, Issue 4, April 2012.

[6] S. Ghazi, K. Mashloosh. Influence of heat treatment on resistance of wear and mechanical properties of die steel kind D3. American Journal of Scientific and Industrial Research, 2015, 5(2): 33-40.

[7] M. Orecny, M. Bursk, M. Sebek, L. Falat. Influence of hardness matrix and carbides in combination with nitridation on abrasive wear resistance of X210Cr12 tool steel. Metals, 2016, 6,236.

[8] J. Bressan, D. Kohls. Rotation bending fatigue test of PH-42 steel plasma nitrided. 13th international conference on fracture, June 16-21, 2013, Beijing, China.

[9] ASTM Metals Hand Books, 10th Edition, Volume (1), Page 639.

[10] T. Nykiel, T. Hryniewicz, Effect of high temperature heating on chemical change in M_7C_3 carbides of AISI D2 tool steel. International Letters of Chemistry and Physics and Astronomy 17 (3) (2014) 258-271.

SRJMET

Scientific Research Journal for Metal Engineering and Technologies ISSN:399-2017
Volume No.01 Issue No. 01, PP 87 - 105 01. Jan.2018

Effects of Low Constraint Conditions on Fracture Toughness and Failure Assessment

Osama Terfas[a], Reda Areibi[b] and Abdulbaset Kraima[b]

a) Department of Marine and Offshore Engineering. University of Tripoli

b) Department of Mechanical and Industrial Engineering. University of Tripoli

O.Terfas@uot.edu.ly

Abstract

The reduction of crack tip stresses due to specimen thickness, crack depths and across the thickness was examined using fracture mechanics testing and finite element analysis. This reduction of crack tip stresses was correlated with the fracture resistance. A correlation between in-plane, out-of-plane constraint, and the constraint through the thickness with fracture toughness was established. It was observed that testing deeply thin geometries provide similar fracture resistance to that measured on shallow thick geometries. The study revealed that fracture toughness data determined from different specimens' thicknesses can now be obtained by testing only a series of specimens of one size, inherently less material and short time are required. The application of this research findings of geometries with low constraint conditions exist in non-standard fracture testing are economically beneficial in fitness-for-service (FFS) assessment as it allows to define precisely the failure condition and to avoid the unnecessary replacement while maintaining component integrity.

Key words: Constraint, fracture toughness, fracture resistance, failure assessment.

الملخص

تم إجراء اختبارات ميكانيكا الكسر واستخدام طريقة تحليل العناصر المتناهية لدراسة آلية الانخفاض في الاجهادات على مقدمة الشروخ نتيجة لاختلاف السمك، عمق الشرخ، وخلال الانتقال عرضيا على طول السمك. حيث تم إنشاء علاقة بين هذا الانخفاض في قيمة اجهادات الشروخ مع مقاومة الكسر، بالإضافة إلى العلاقة بين تأثير السمك وعمق الشروخ. حيث تم ملاحظة ان قيم مقاومة الكسر المتحصل عليها من اختبار العينات الرقيقة السمك ذو الشروخ العميقة متساوية مع تلك المتحصل عليها من العينات السميكة ذو الشروخ قليلة العمق. كما

بينت الدراسة انه يمكن الآن الحصول على قيم مقاومة الكسر من خلال اختبار نوع واحد من العينات بدلا من اختبار العديد من العينات بمختلف السماكات وأطوال الشروخ. وهذا بدوره يقلل من عدد عينات الاختبار اللازمة والتقليل من زمن الاختبارات. كما أظهرت الدراسة ان متانة الكسر تتأثر بشكل كبير جدا بقيمة وحالة الاجهادات وليس بحالة الانفعال. لذا يمكن الاستفادة اقتصاديا من نتائج هذه الدراسة عمليا في تقيم المكونات الهندسية (ملائم للخدمة) حيث إنها تحدد وتقيم بدقة حالة الفشل للقطع الهندسية التي بها شروخ وتجنب عمليات الإحلال غير الضرورية مع المحافظة على سلامة تلك القطع للقيام بوظيفتها طيلة فترة الخدمة.

1. Introduction.

Fracture toughness data derived from fracture mechanics testing described in ASTM E1737 and BS7448 standards are necessarily conservative as they are based on thick-deeply cracked geometries. Consequently, this provides lower bound material resistance to ductile fracture that is expressed in terms of fracture toughness and resistance curves, J-Δa. In reality, many engineering components have thin-walls and may contain shallow cracks that exhibit low stress levels. Therefore, fracture toughness data relevant to shallow cracked geometries and to the thickness of the particular geometry is needed in order to provide an accurate margin of safety and to reduce the cost of unnecessary replacement.

Fracture toughness tests for low constraint conditions for ductile materials showed that single edge cracked tension test and shallow cracked bend test can be used to create constraint based J-R curves (Zhu 2015). Han et al. (2016) observed that notch tip radius and the crack depth have significant effects on crack tip constraint levels, inherently on fracture toughness. Kim (2003) showed that in small scale yielding conditions deep cracked geometries maintain high crack tip constraint and the effect of thickness on the crack tip constraint can be ignored. However, in shallow square specimens the constraint reduces at much lower load levels. Hancock et al. (1993) observed that there is a significant effect of constraint on toughness after crack initiation, and there is a strong effect of constraint on the slope of the ductile resistance curves. Ostby (2007) pointed out that the J-R curves reveal little dependence on the

specimen size for small amount of ductile crack growth. The size effect becomes more significant with further crack growth in small specimens and increases in low hardening materials. It was observed that J-R curves for HY80-Steel are strongly dependent on the crack size, and shallow cracks provide higher resistance curves, and the fracture toughness at initiation, J_{Ic}, is weakly dependent on the crack tip constraint, and the critical fracture toughness after initiation is strongly dependent on the level of constraint (Zhu and Joyce 2007). The effect of thickness in small specimens (w=20, B=10mm) on the J-Δa curves under ductile tearing is relatively small compared to the increase in toughness for larger crack extensions (Smith, 2008). Larger specimens (w=80, B=40) exhibited a significant reduction of the slope of the J-Δa curve, and are less resistant to ductile tearing.

The aim of this work is to examine the mechanisms of loss of crack tip stresses due to the thickness, crack depths and travelling across the thickness using fracture mechanics testing and finite element analysis. It is desired to correlate the reduction of crack tip stresses with the fracture resistance. This work also intends to create a correlation between in-plane, out-of-plane constraint and the loss of constraint through thickness with fracture toughness in order to construct the material failure curve.

2. Research methodology.

1- A series of fracture mechanics specimens with standard and nonstandard geometries with different crack depths and thicknesses were prepared and machined.
2- A fatigue pre-cracking test was prepared to obtain the desired crack-depth ratio.
3- A three-point bending test was conducted for all prepared specimens.
4- Measurement of the fatigue crack lengths and the ductile crack extensions was conducted.
5- A 3-dimensional finite element modelling for all specimens tested was performed.
6- The fracture testing data was correlated with finite element modelling data to obtain full fracture mechanics data.

SRJMET

Scientific Research Journal for Metal Engineering and Technologies ISSN:399-2017
Volume No.01 Issue No. 01, PP 87 - 105 01. Jan.2018

7- Data was analysed and discussed.

3. Geometry and materials data.

The geometry examined was an edge cracked bend specimen is shown in Figure 1. The geometry dimensions of deeply cracked thick, thin specimens, and shallow cracked specimens are shown in Table 1. Side grooved and non-side grooved geometries were used. For side-grooved specimens the side groove with an angle of 45˚ was cut to a depth of 10 % of the thickness on each lateral face to obtain 80% net thickness of the full thickness.

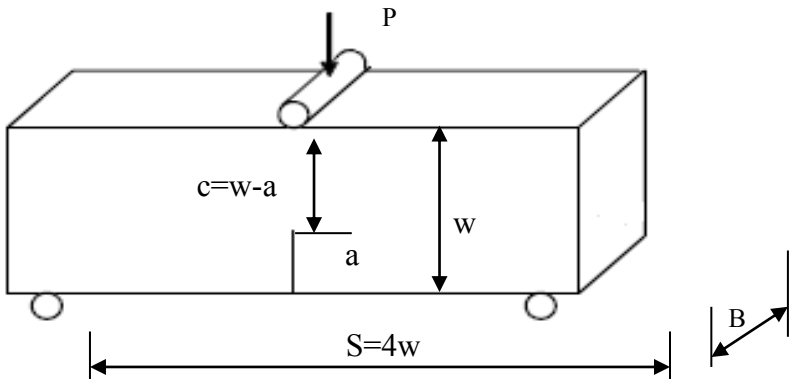

Figure 1: Geometry of a single edge cracked bend specimen used.

Table 1: The geometry of test specimens.

Specimen type	Dimensional (mm)			Non-dimensional		
	w	a	B	a/w	B/w	B/(w-a)
1-Deep cracks (Standard geometry)	50	25	25	0.5	0.5	1
2-Deep cracks (Non-Standard geom.)	50 50 50	25 25 25	10 5 3	0.5 0.5 0.5	0.2 0.1 0.06	0.4 0.2 0.12
3-Shallow cracks (Non-Standard geom.)	28 30	3 5	25 25	0.1 0.16	0.89 0.83	1 1

The tensile test for the mild carbon-manganese steel was performed using a specimen diameter of 5.64 mm and a 32 mm gauge length at 20˚C. The true stress

versus true strain curve was derived from the engineering stress-strain relation as shown in Figure 2.

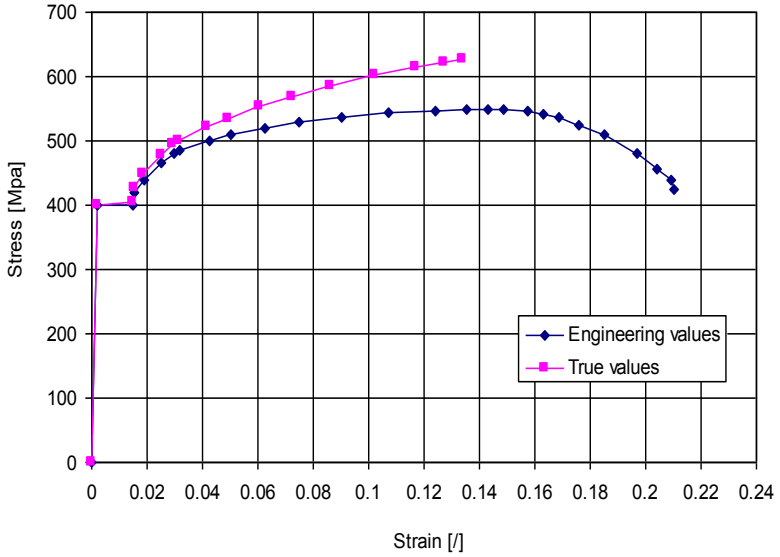

Figure 2: Stress-strain curve for the material used in the fracture tests.

The power-low equation of Ramberg-Osgood was used to determine the strain hardening coefficient by matching its approximations with the true stress-strain curve:

$$\varepsilon = \frac{\sigma}{E} + 0.002\left(\frac{\sigma}{\sigma_y}\right)^n \quad \text{..... (1)}$$

Where, ε is the strain, σ is the stress, E is Young`s modulus, σ_y is the yield stress, and n is the strain hardening coefficient.

It is shown in Figure 3 the material behaviour can be considered as a low hardening with n=10 which is the closest approximation to the true stress-strain curve. The

related mechanical properties of this mild carbon-manganese steel are shown in Table 2.

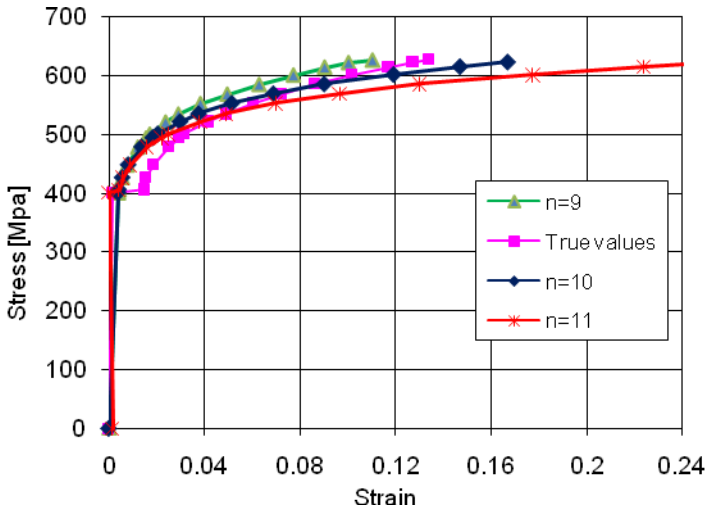

Figure 3: Stress-strain curve versus Ramberg-Osgood approximation equation.

Table 2: Mechanical properties of the mild carbon-manganese steel used.

Property	Hardening exponent	Young's modulus	Poisson's ratio	Yield strength	Ultimate tensile stress
Symbol, Unit	n	E, GPa	v	σ_0, MPa	σ_{uts} , MPa
	10	210	0.3	400	626

4. Test preparation.

Fracture mechanics samples were cut from a 25mm thick rolled plate. Samples were notched with a cutter such that the crack plane contained the rolling direction and the short transverse direction, T-L. Samples were first fatigue pre-cracked in three points bending according to BS 7448. During the fatigue pre-cracking the load was periodically reduced with fatigue crack growth to keep the maximum stress intensity factor below 30MPa√m. Fatigue precracking was done at room temperature using a hydraulic machine at a frequency of 3-4Hz and a stress ratio (R) of 0.1. This was repeated until the desired crack depth was obtained.

SRJMET
Scientific Research Journal for Metal Engineering and Technologies ISSN:399-2017
Volume No.01 Issue No. 01, PP 87 - 105 01. Jan.2018

5. Test procedure .

Fracture tests were performed on a universal testing machine equipped with three point bending set-up as shown in Figure 4. A multiple specimen technique was used, where a set of 4 to 6 specimens for each geometry were tested. Samples were tested under displacement control at a cross-head speed of 0.5mm/min. The load line displacement was measured by the movement of the crosshead. Each specimen was subjected to a chosen amount of displacement and the amount of crack extension associated with this loading was measured after the test. The first specimen was used to determine the full force-displacement curve and the test was stopped at the maximum load. Subsequent tests were stopped at progressively smaller clip-gauge displacements. All tests were performed at room temperature and ambient conditions.

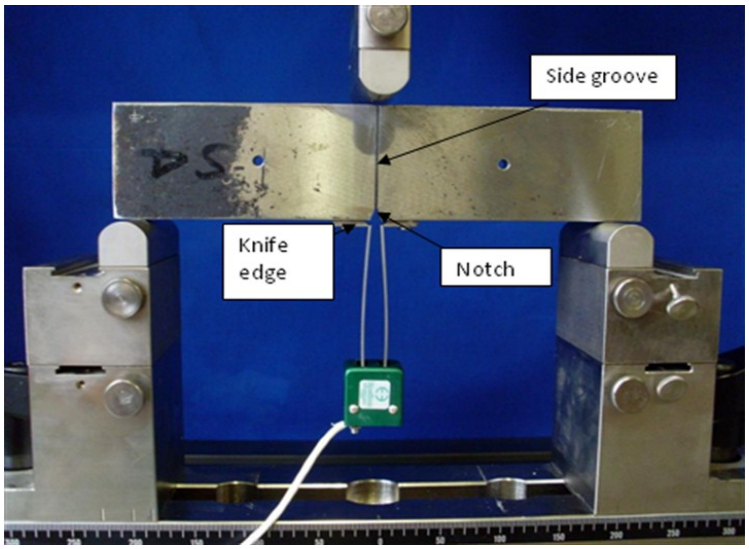

Figure 4: A specimen with a clip gauge in the three points bend test.

To measure the notch opening displacement a clip gauge was placed on the sample using a set of 3mm high knife edges. During the test, the applied load (P) and load-line displacement (LLD) curve as well as the load-notch opening displacement (V) curve were recorded. Three experimental load and load-line displacement curves are shown in Figures 5, 6 and 7 for thick (B/w=0.5), thin (B/w=0.2), and very thin (B/w=0.1) specimens, respectively.

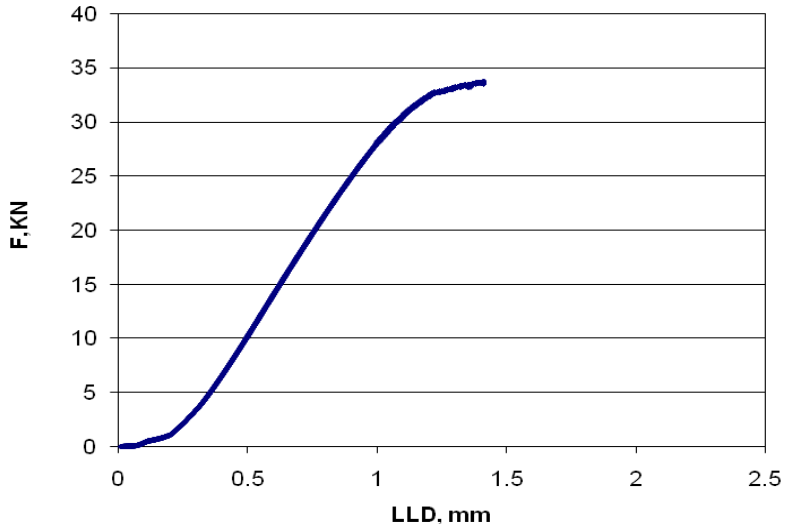

Figure 5: Load versus load-line displacement for thick cracked specimen (B/W=0.5).

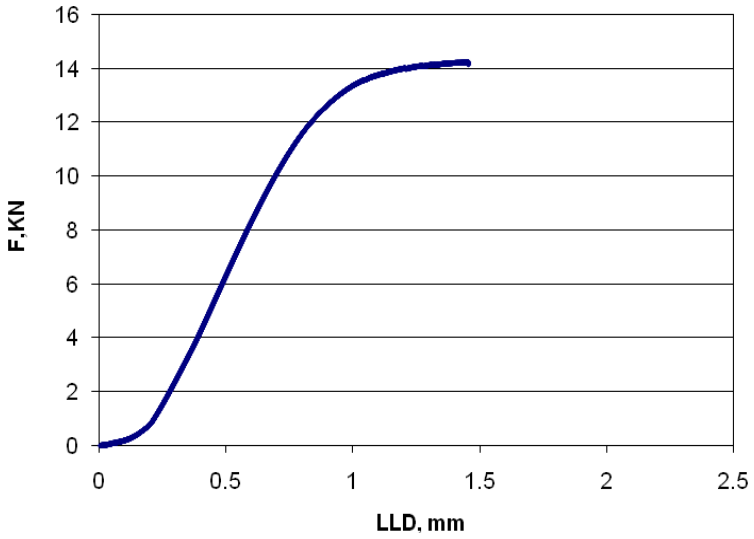

Figure 6: Load versus load-line displacement for thin cracked specimen (B/W=0.2).

SRJMET

Scientific Research Journal for Metal Engineering and Technologies ISSN:399-2017
Volume No.01 Issue No. 01, PP 87 - 105 01. Jan.2018

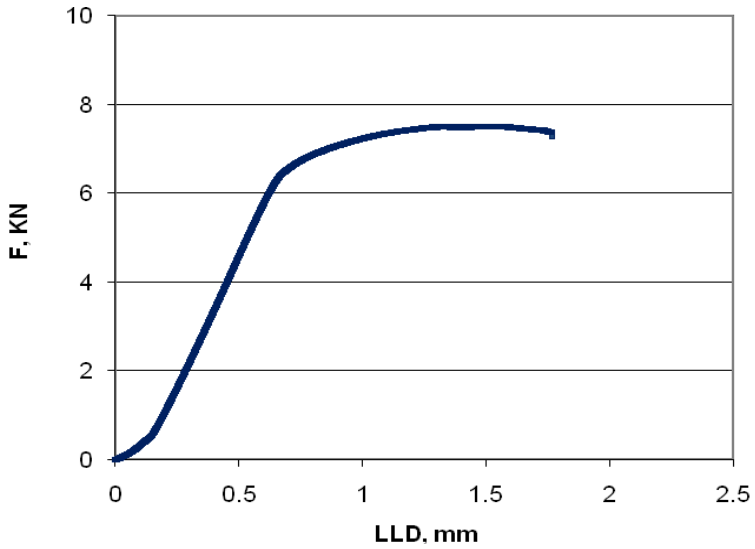

Figure 7: Load versus load-line displacement for very thin cracked specimen (B/W=0.1).

The plastic component of the notch opening displacement (Vp) was measured graphically at the termination of the test. The plastic energy absorbed in the material (U_p) was determined for each test by measuring the area under the load-displacement curves. The experimental J-integral was calculated in accordance with British Standard BS 7448:

$$J = \left[\frac{F.S}{B.W^{0.5}} \times f\left(\frac{a_0}{W}\right)\right]^2 \frac{\left(1-v^2\right)}{E} + \frac{2.U_p}{B(W-a_0)} \qquad \text{.....(2)}$$

Where, F is the applied load, S is the bending span, B is the thickness, W is the width of the specimen, V is poison's ratio, E is the Young`s modulus, a_0 is the initial crack, Up is the plastic energy, and $f(a_0/W)$ is the geometry factor.

6. Measurements of the initial crack length and the ductile crack extension.

After the test, the specimens were cooled in a liquid nitrogen bath and broken open, and the initial fatigue pre-crack length a_0 and stable crack growth Δa were measured at nine equally spaced points through the thickness. This was done first by averaging the two side surface crack lengths, and then averaging this value with the

other seven points and dividing by eight. The ductile crack extension was measured from the end of the fatigue pre-crack to the final extension, at the same nine equally spaced points along the crack front and averaged in the same manner. The original length of the fatigue crack a_0 for all specimens was in the range of 0.47-0.55w. A sample of the fracture surface of a plane sided specimen is shown in Figure 8.

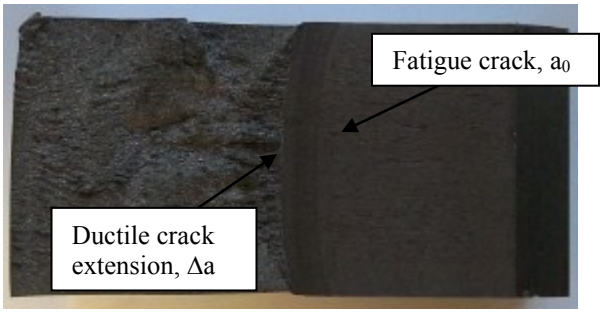

Figure 8: Fracture surface of a test sample.

7. Finite element model .

Finite element analysis was conducted to obtain accurate crack-tip stress fields. The crack was modelled as a sharp crack, and the element type of continuum three-dimensional with reduced integration, C3D8R was used. Due to symmetry conditions, only a quarter of the specimen was modelled and appropriate symmetry boundary conditions were applied on the planes of symmetry as shown in Figure 9. The J-integral was evaluated using a contour defined in the far field where J-integral is still path-independent. The mean stress was calculated across the thickness at a distance $2J/\sigma_0$ where J is local J-integral.

SRJMET
Scientific Research Journal for Metal Engineering and Technologies ISSN:399-2017
Volume No.01 Issue No. 01, PP 87 - 105 01. Jan.2018

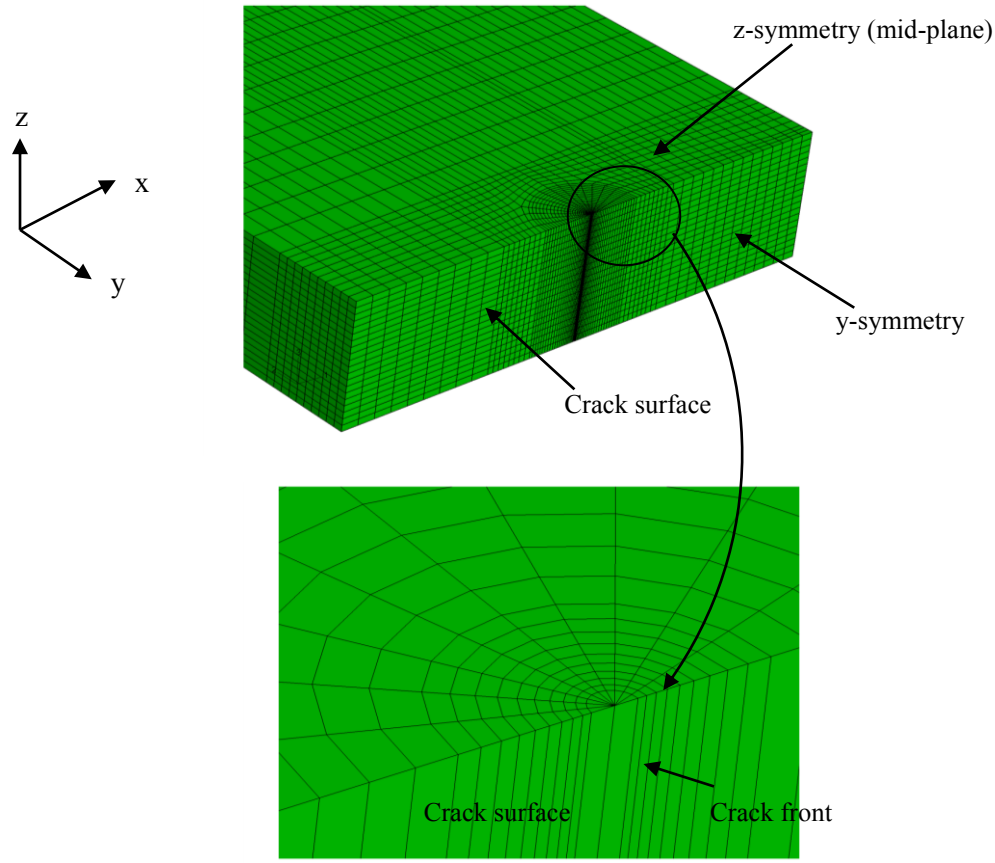

Figure 9: Finite element model for an edge cracked bend bar.

The values of mean stress and J-integral are presented in Figures 10 to 13, and theses values were used to construct the fracture resistance curves. Figure 10 shows a high mean stress along the crack front for thick non-side grooved geometries. This high mean stress maintained from the mid-plane to quarter-plane. At the free surface the stresses cluster around the plane stress solution. For a thin cracked geometry, the mean stress maintained high levels of constraint only at low deformation levels at the mid-plane but rapidly reduced towards the free surface as shown in Figure 11.

SRJMET

Scientific Research Journal for Metal Engineering and Technologies ISSN:399-2017
Volume No.01 Issue No. 01, PP 87 - 105 01. Jan.2018

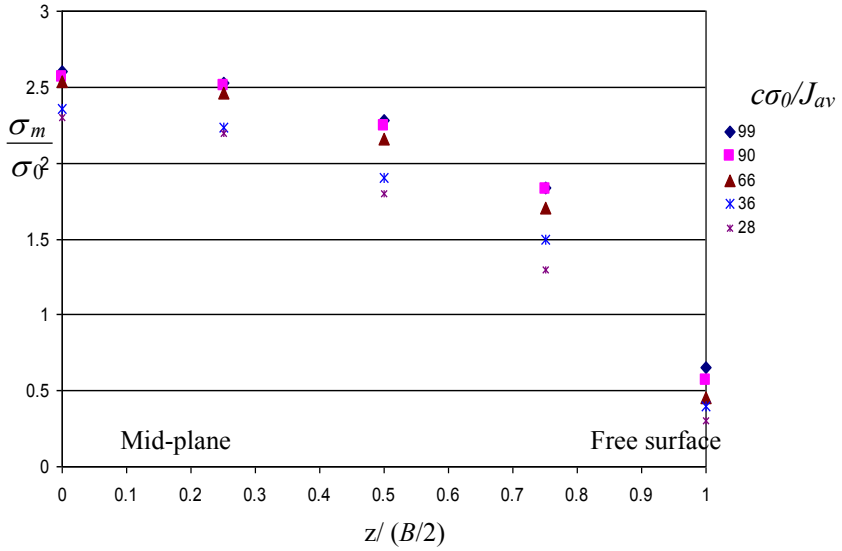

Figure 10: The mean stress along the crack front for thick non-side grooved specimens (B/w=0.5).

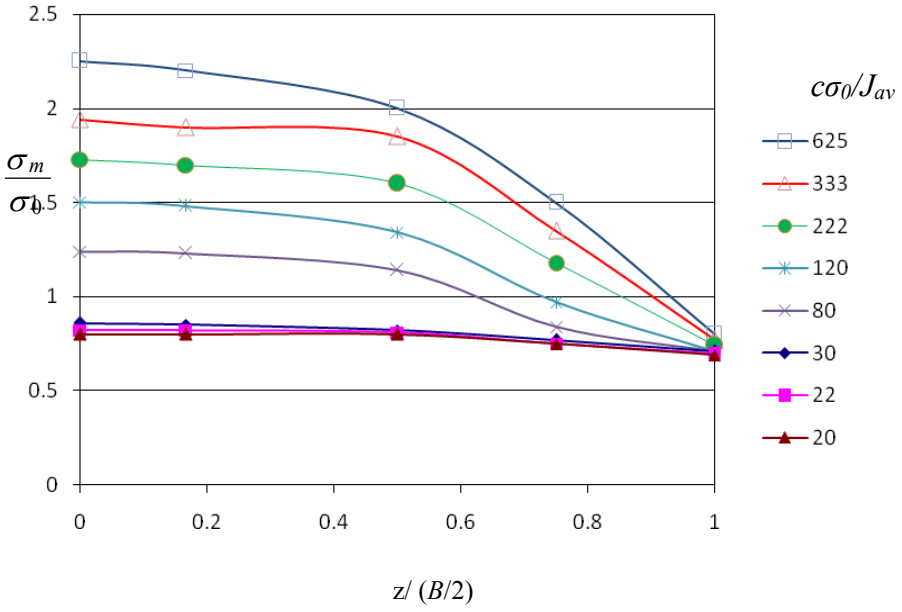

Figure 11: The mean stress along the crack front for thin non-side grooved specimens (B/w=0.06).

Figure 12 shows non-dimensional J-integral ($J/c\sigma_0 e_0$) along the crack front from the mid-plane to the free surface for thick non-side grooved geometry, where e_0 is taken as σ_0/E. A big variation was observed in J-integral values across the thickness and the maximum value at the mid-plane decreased gradually towards the free surface. For

SRJMET

Scientific Research Journal for Metal Engineering and Technologies ISSN:399-2017
Volume No.01 Issue No. 01, PP 87 - 105 01. Jan.2018

thin specimen, the J-integral distribution decreased sharply from the maximum value at the mid-plane to the minimum at the free surface at high deformation levels $c\sigma_0/J_{av} \leq 30$ as shown in Figure 13.

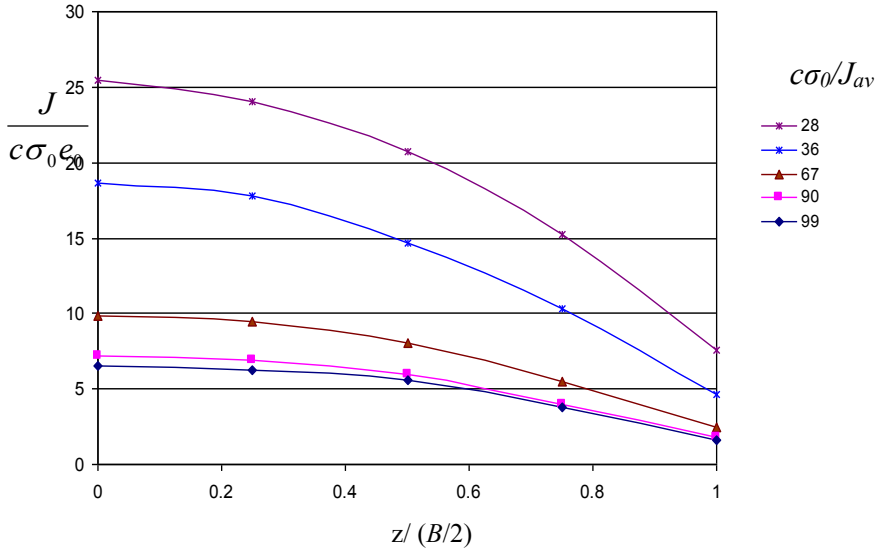

Figure 12: J-integral along the crack front for thick non-side grooved specimens (B/w=0.5).

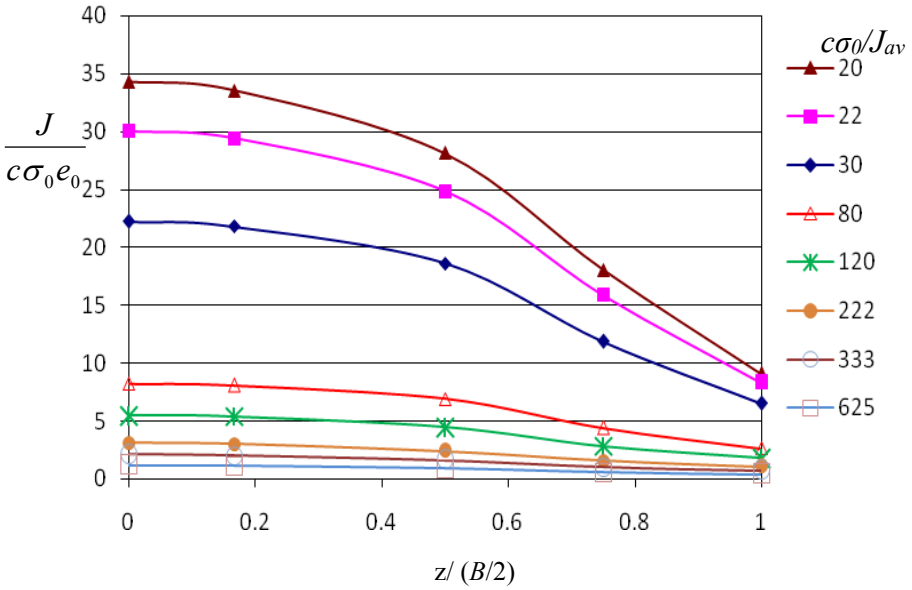

Figure 13: J-integral along the crack front for thin non-side grooved specimens (B/w=0.06).

8. The fracture resistance curves (J-Δa curves) .

The fracture resistance curves of deeply cracked thick and thin side grooved specimens are shown in Figure 14. The fracture toughness (J) for each test specimen is

plotted versus the crack tip extension Δa. It is shown that low resistance curve is associated with thick specimens, while a further decrease in thickness to (B/w=0.1) results a significant increase in fracture toughness. This means the fracture toughness J_{Ic} is dependent on the specimen thickness with thin specimens having a higher fracture toughness.

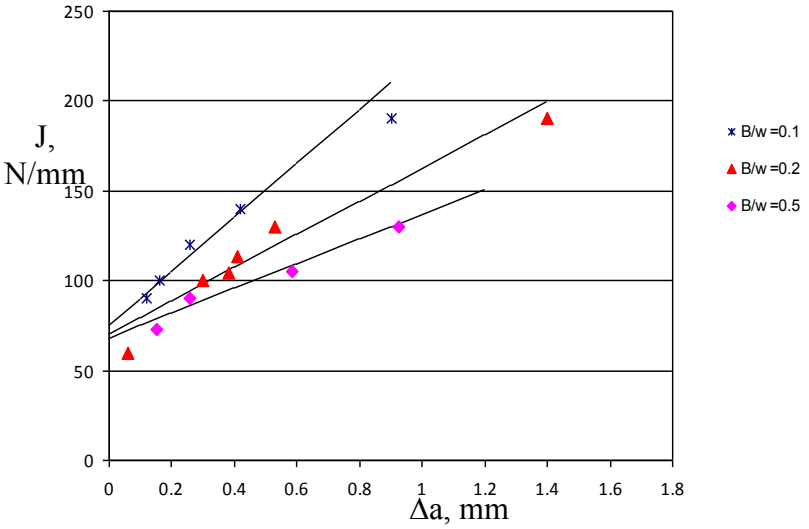

Figure 14: The J-Δa curve for deeply cracked thick and thin side grooved specimens.

Shallow cracked specimens with side groove showed a large increase in ductile fracture resistance curve, inherently higher fracture toughness as shown in Figure 15. High constraint levels associated with deep cracked specimens tended to cause a lower crack growth resistance curve compared to shallow cracked specimens.

SRJMET
Scientific Research Journal for Metal Engineering and Technologies ISSN:399-2017
Volume No.01 Issue No. 01, PP 87 - 105 01. Jan.2018

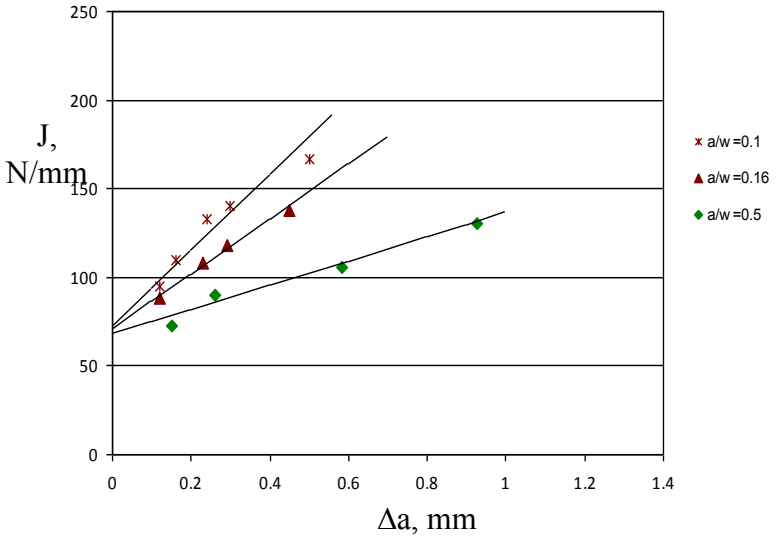

Figure 15: The fracture resistance curve for deep and shallow side grooved specimens.

Local J-values across the thickness of the specimen and associated ductile crack extension were used to construct J-Δa curve as shown in Figures 16 and 17, for deeply thick and thin non-side grooved specimens, respectively. The points shown represent several planes across the thickness starts from mid-plane (x/B=0mm) where both the constraint and J-integral are largest, and reduces through the thickness and become smallest at the free surface (x/B=0.5mm). At mid-plane high constraint levels maintained cause lower resistance curves than at the free surface where higher resistance curves associated with low crack tip constraint.

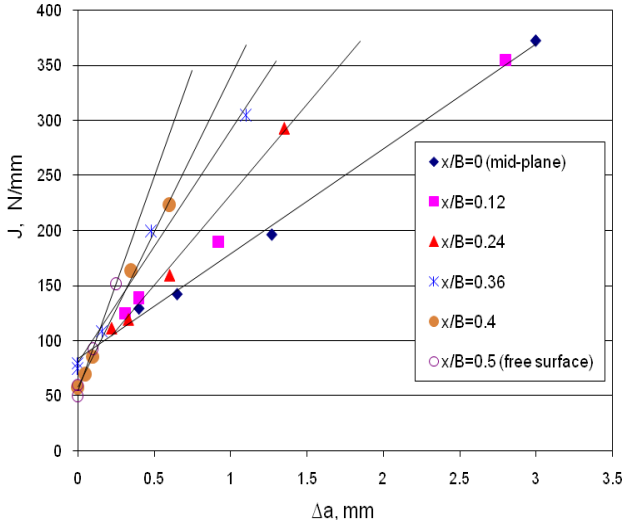

Figure 16: J-Δa resistance curve for thick non-side grooved specimens (B/w=0.5) across the thickness.

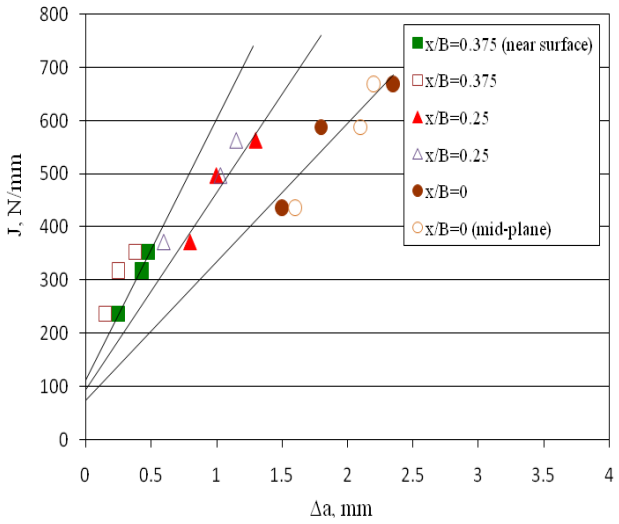

Figure 17: J-Δa resistance curve for thin non-side grooved specimens (B/w= 0.06) across the thickness.

9. Discussion.

In three-dimensional problems crack tip constraint can be lost due to in-plane effects, global bending and out-of-plane effects. As a result, an increase in toughness associated with thin specimens and shallow cracked specimens was observed. Similarly, lower resistance curve was obtained at mid-plane than the resistance curve for the free surface. It was observed that fracture toughness at initiation Δa=0 is constraint independent. However, for more practical crack extensions Δa=0.4mm the effect of loss of constraint was obvious and has more effect on the slope of ductile resistance curves. Therefore, it is of interest to correlate constraint loss with the slope of the resistance curve in terms of the tearing modulus defined as $T_R=\partial J/E\partial a$ as shown in Figure 18. It can be seen that fracture data points obtained from various cracked geometries lie on one curve which means the toughness does not depend on the state of strain. Therefore, there is no need to reduce the thickness of the specimen to obtain fracture data as this can be obtained by examining standard fracture mechanics specimens by measuring the crack extension at different points through thickness. This in practical terms suggests use of constraint dependent toughness measured on shallow

cracked samples to be used on thin structures with deep cracks. These observations also eliminate the excess use in fracture samples and only one size of non-side grooved specimens can be used. Inherently this saves material and shortens time required to prepare the testing.

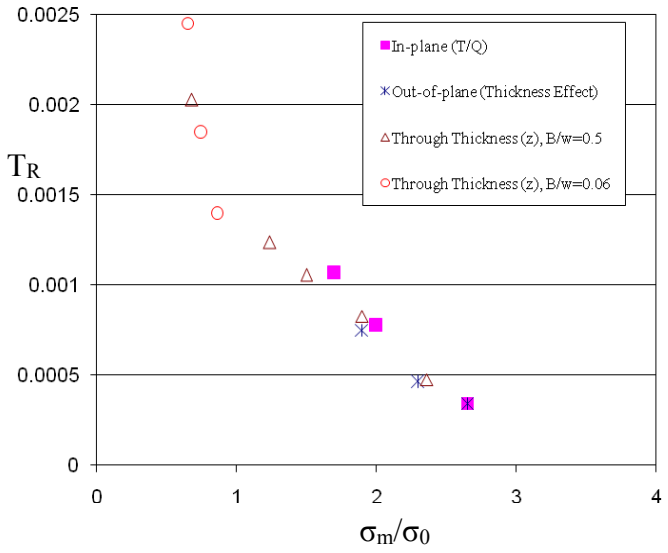

Figure 18: Tearing modulus as a function of mean stress.

Figure 19 shows the critical fracture toughness as a function of constraint quantified by mean stress at crack extensions of $\Delta a=0$ and 0.4mm. The figure shows that at a point where there is no crack extension the effect of constraint on toughness is insignificant. However, for larger crack extensions ($\Delta a=0.4$mm) the fracture toughness becomes geometry dependent and constraint effect becomes highly significant. The curve shows the loss of constraint due to in-plane or out-of-plane effect causes a similar and a significant increase in toughness.

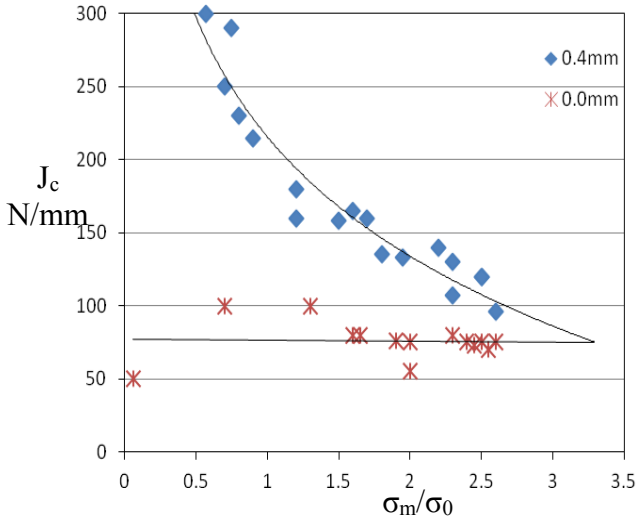

Figure 19: Critical fracture toughness as a function of crack tip mean stress.

10. Conclusions .

The loss of crack tip stresses due to in-plane, out-of-plane and through thickness was correlated to the ductile tearing modulus. It was observed that material fracture data can be obtained using one specimen size due to the variation of the constraint levels exists across the thickness which is consistent with the variation of the local J-integral, inherently less material and short time are required. This investigation emphasised that fracture toughness is strongly influenced by the level of stress and it is independent of state of strain. The application of this research findings of geometries with low constraint conditions are economically beneficial in fitness-for-service assessment as it allows to define the margin of safety precisely and to avoid the unnecessary replacement.

References .

1. ASTM E1737, 1998. Standard test method for J-integral characterization of fracture toughness, *American Society for Testing and Materials*.
2. BS7448, 1997. Method for determination of fracture resistance curves and initiation values for stable crack extension in metallic materials, *British Standard Institution*, London.

3. Han, J.J., Larrosa, N. O., Ainsworth R. A., Kim Y. J. 2016. *The use of SE(T) specimen fracture toughness for FFS assessment of defects in low constraint conditions*, 21st Euorpean Conference on Fracture, Italy.

4. Hancock, J.W., Reuter, W.G., Parks, D.M. 1993. Constraint and toughness parameterised by T. Constraint effect in fracture. *ASTM STP* 1171, Philadelphia.

5. Kim,Y., Chao, Y. J., Zhu, X. K. 2003. Effect of specimen size and crack depth on 3D crack-front constraint for SENB specimens. *International Journal of Solids and structures*.

6. Kim,Y-Jae., Kim, J. S., Cho, S. M., Kim, Y-Jin. 2004. 3-D constraint effects on J testing and crack tip constraint in M(T), SE(B),SE(T) and C(T) specimens: numerical study. *Engineering Fracture Mechanics*.

7. Ostby, E., Thaulow, C., Zhang, Z. L. 2007. Numerical simulations of specimen size and mismatch effects in ductile crack growth-Part I: Tearing resistance and crack growth paths. *Engineering Fracture Mechanics*.

8. Smith, D. J., Swankie, T. D., Pavier, M. J., Smith M. C. 2008. The effect of specimen dimensions on mixed mode ductile fracture, *Engineering Fracture Mechanics*.

9. Zhu, X-K. 2015. *Advances in Fracture Toughness Test Methods for Ductile Materials in Low Constraint Conditions*, 14th International Conference on Pressure Vessel Technology, Shanghai, China.

10. Zhu, X-K., Joyce, J. A. 2007. J–Resistance curve testing of HY80 steel using SE(B) specimens and normalization method, *Engineering Fracture Mechanics*.

SRJMET

Scientific Research Journal for Metal Engineering and Technologies ISSN:399-2017
Volume No.01 Issue No. 01, PP 106 - 119 01. Jan.2018

Effects of Friction Welding Parameters on Mechanical Properties of Alloy Steel Din 1.2714 Welded Joint

Ibrahim Altoumi[a] and Khaled Alwaer[b]

Institute of Technical Science, Algarapulli, Libya

[a] ibrahimahmed@gmail.com, [b] Khaled_aa2001@yahoo.com

Abstract

The friction welding process is described as way of joining materials together using heat resulted from friction as well as pressure. The mechanical power is transformed in heat by using rotation of one part of the two work piece parts while the other part is fixed , then the two surfaces are heated as a consequence of dry friction then the fixed surface squeezed in order to obtain the joint. In this paper friction welding was carried out on alloy steel material (DIN 1.2714). The welded material samples were chosen from two different material conditions, the first welded samples taken as received material condition, the other samples were taken from the material after annealed condition. In both welded material conditions, same friction welding parameters are applied. In order to find the proper welding parameters which improve both the hardness and strength, different welding cases with different parameters were applied. To investigate the mechanical properties of welded material condition, the welded samples were tested using Vickers hardness test. Comparing was made in both welded conditions and the results correlated with the tests results of the original material before welding. The results shows improving in welded joint properties were obtained at suitable welding parameters and for each welded condition response to different welding parameters cases.

SRJMET

Scientific Research Journal for Metal Engineering and Technologies ISSN:399-2017
Volume No.01 Issue No. 01, PP 106 - 119 01. Jan.2018

Key words: friction welding, mechanical properties, rotation speed, welding parameters.

1. Introduction .

Friction welding (FRW) in this simple form involves two axially reached parts. When one part is rotated, the other stationary part is advanced to make pressure contact. Axial force then increases to generate the frictional heat necessary for welding at the abutting surfaces in order to form a solid-state joint. Friction welding can be divided into two major process variations, depending on the manner by which rotational energy is converted into frictional heat. The first process direct drive FRW has been used commercially since the 1940 **[1].** It requires constant energy from a source for any desired duration. The second process, inertia drive FRW, which was developed in the early 1960, uses the kinetic energy stored in a rotating flywheel. At present there is a product evaluation that must rely on the control of the process and the machine that is used to produce the welds. In direct drive FRW, both rotational speed and axial force affect axial shortening or upset in addition to the axial force affect axial shortening or upset in addition to the mechanical properties of the weld part. There can be a correlation between the upset and the quality of the weld. Further, upset in phase 2 heating increases almost linearly with time. The upset of this phase often called friction burn off, and its rate the friction burn off rate, have been believed to control weld quality. Indeed some researchers use burn off instead of duration of rotation as a welding parameter. In inertia drive FRW, because duration of rotation is not preset but controlled by the three welding parameters of the total upset instead of friction burn off, is supposed to indicate weld quality. This presumes that the same amount of kinetic energy and axial force will produce the same amount of upset at the end of the process (given the same materials and cross sections) [1]. (Tool steels are the alloys

used to manufacture the tools, dies, that shape form, and cut other materials, including steels, nonferrous metals, and plastics [2]. The tool steels are difficult to welding using conventional welding processes due to grade of hardness [3]. DIN 1.2714 Alloy Steel Used sleeves for extrusion process and moulds casting. In this paper study of how the mechanical properties of friction welded alloy steel DIN1.2714 can be affected by changing welding parameters. DIN 1.2714 Alloy Steel according to (Germany Deutsches Institut for Normung) high resistance to thermal shock and to heat cracking, excellent mechanical characteristics in cold state and Good mechanical characteristics in hot condition in addition to Excellent toughness in both hot and cold condition and in status [4].

2. Experimental work .

2.1. Work Piece Material

The used material for this study is Din 1.2714 according to Germany Code, the chemical composition of this material as shown in Table 1.

Table 1 Chemical composition of Work piece material.

C	Si	S	P	Mn	Ni	Cr	Mo
0.5839	0.2785	0.0079	0.0093	0.8395	1.5273	1.1206	0.4801
V	Cu	W	Ti	Sn	Pb	Zn	Fe
0.0914	0.1044	0.0153	0.0033	0.0055	0.0047	0.0071	rest

2.2 Friction Welding Machine.

The welding was done in the engineering research centre, welding branch, Tajura. The specifications of the mechanical friction welding used for welding the chosen material are the machine made by UK/ Thomson Company which are used for bars and pipes welding with maximum pressure (140 bars) and (2500 rev/min) maximum rotational speed.

SRJMET
Scientific Research Journal for Metal Engineering and Technologies ISSN:399-2017
Volume No.01 Issue No. 01, PP 106 - 119 01. Jan.2018

2.3. Sample Preparation and Welding.

In this work, samples were cut from selected material pipe have size (30mm diameter, 200mm long and 5mm thickness) using saw cut machine and wire cut machine then machined to proper way for welding. Eleven samples were cut, five of them were heat treated (annealed) Heat treatment was carried out by heating the piece to 700 ° C and maintaining it at that temperature for approximately 20 hours. It cooled slowly inside the oven.

Friction welding process were applied on the as received and after annealed specimens, for each specimen in both material conditions change of one or two parameter which are related to friction welding parameters was selected, in the purpose to find better hardness result. The selected parameters for friction welding before and after annealing are shown in Table 2 and Table 3 respectively. Those parameters are friction time, friction pressure, rotation speed and forging pressure.

Table 2 Designed various parameters. (Before annealing)

series	Friction Time (sec)	Forging Pressure(bar)	Friction Pressure(bar)	Rotation speed(rpm)
1	2	70	30	1500
2	2	70	40	1500
3	2	70	50	1500
4	3	70	60	1500
5	4	70	60	1500
6	6	70	60	1500

Table 3 Designed various parameters (after annealing)

series	Friction Time (sec)	Forging Pressure(bar)	Friction Pressure(bar)	Rotation speed(rpm)
A	2	70	60	1500

SRJMET

Scientific Research Journal for Metal Engineering and Technologies ISSN:399-2017
Volume No.01 Issue No. 01, PP 106 - 119 01. Jan.2018

B	2	70	40	1500
C	2	70	30	1500
D	4	70	60	1500
I	6	70	60	1500

3. Results and Discussion .

3.1 Hardness and Tensile Strength

In this study, the micro hardness test was tested using the Vickers hardness measuring device and tensile strength tacked from standard table. Results were obtained directly from the measuring device The results obtained before the annealing process were shown in the figures (1- 6), and the results obtained after annealing process were shown in figures (7-11). The results show some facts which can be summarized as follows:

A- In Sample 1, 2 and 3 the friction time, speed rotation, forging pressure were constant however, the friction pressure was changed. The low friction pressure gives increases mechanical properties of the alloy steel DIN1.2714.

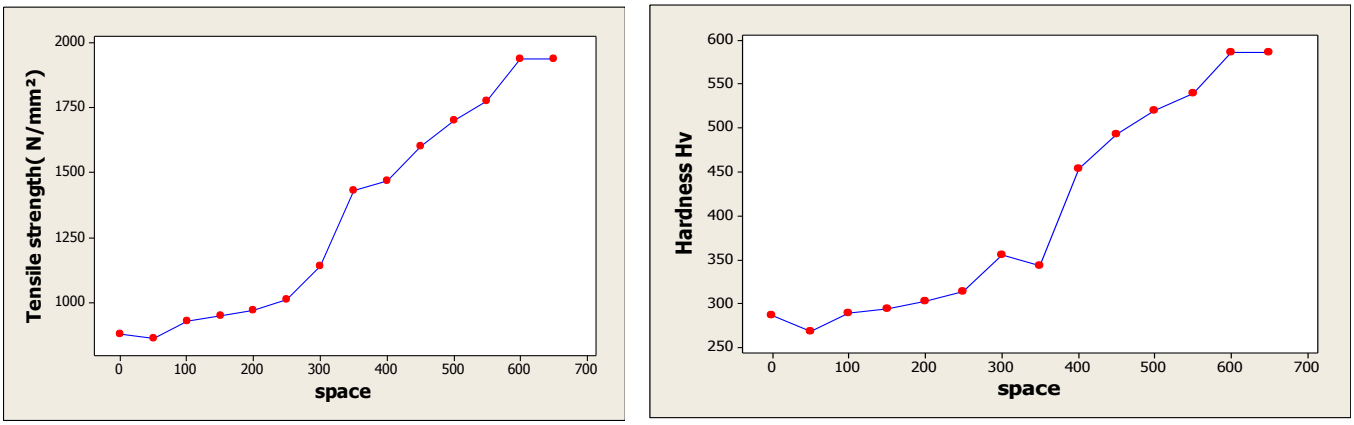

Figure 1 Hardness and tensile strength for Sample 1.(before annealing)

SRJMET

Scientific Research Journal for Metal Engineering and Technologies ISSN:399-2017
Volume No.01 Issue No. 01, PP 106 - 119 01. Jan.2018

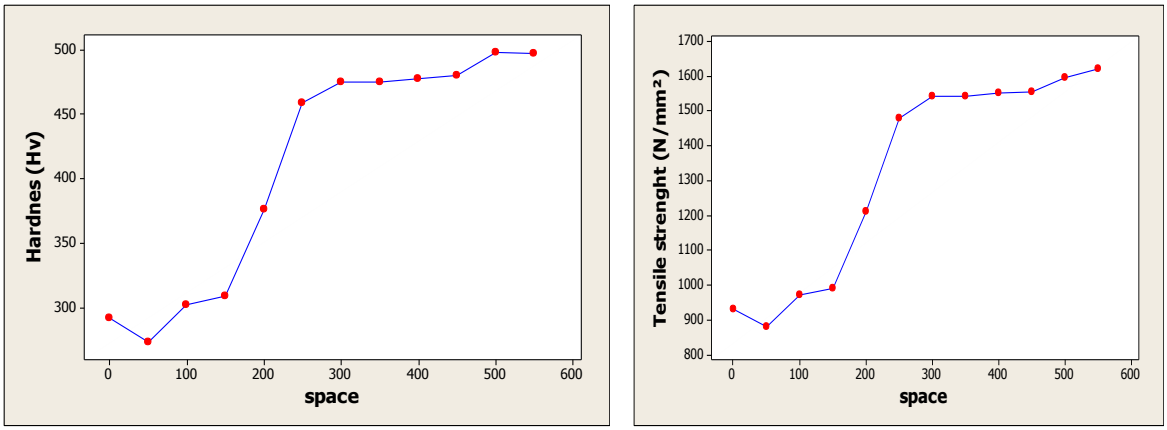

Figure 2 Hardness and tensile Strength for Sample 2. .(before annealing)

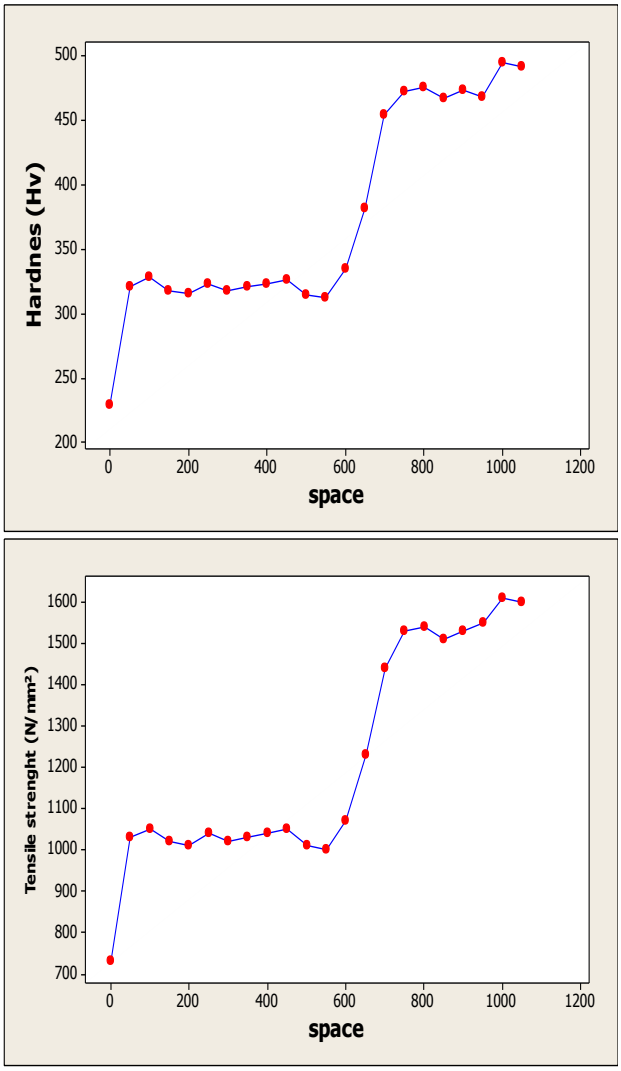

Figure 3 Hardness and tensile Strength for Sample 3.(before annealing)

B- In Sample 4 all the parameters were stabilized then friction time changed a good friction welding was gained because the friction time was low and the friction pressure was still high.

SRJMET

Scientific Research Journal for Metal Engineering and Technologies ISSN:399-2017
Volume No.01 Issue No. 01, PP 106 - 119 01. Jan.2018

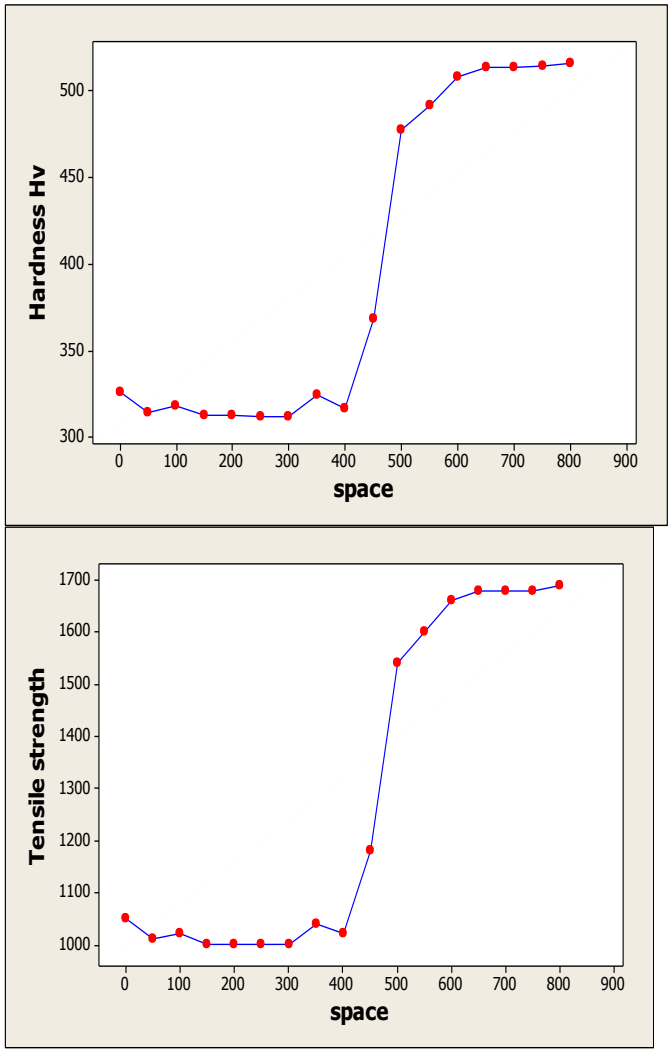

Figure 4 Hardness and tensile Strength for Sample 4.(before annealing)

C- In Sample 5 and 6 the parameters were stabilized and the friction time was changed. The friction time was high and the friction pressure was also still high .The friction time effects the temperature output and controls its diffusion rate. The tensile strength increases along with the increase of friction time.

SRJMET

Scientific Research Journal for Metal Engineering and Technologies ISSN:399-2017
Volume No.01 Issue No. 01, PP 106 - 119 01. Jan.2018

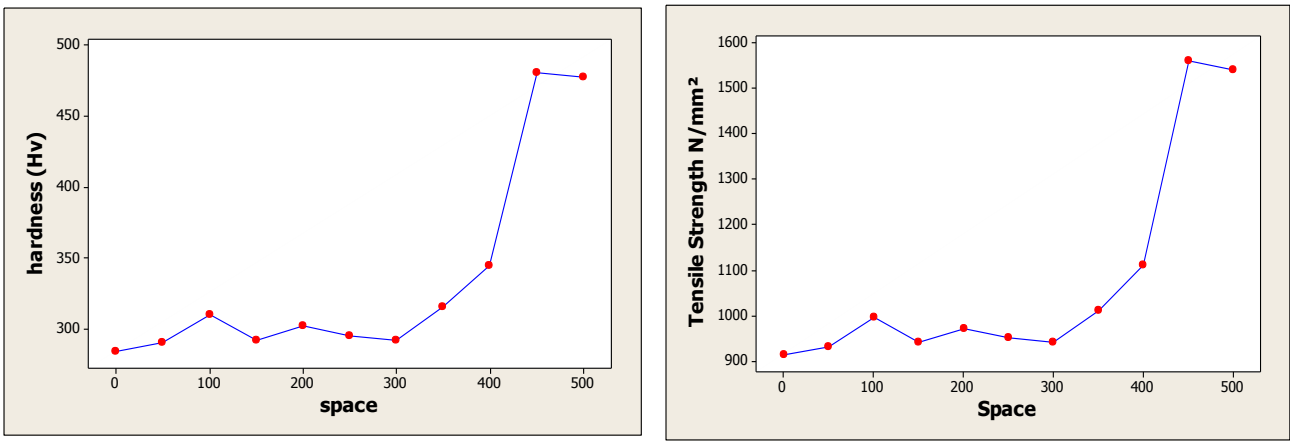

Figure 5 Hardness and tensile Strength for Sample 5 (before annealing)

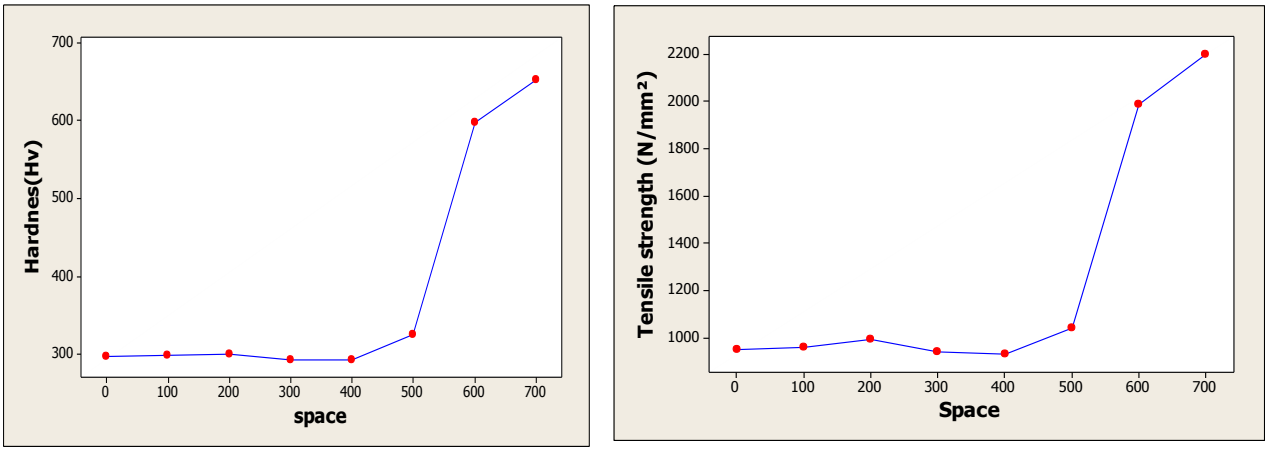

Figure 6 Hardness and tensile for Sample 6. (Before annealing)

D- In Sample A, B, C the parameters were stabilized and the friction pressure was changed.

E- In Sample D the welding friction time increase and friction pressure still constant at high value

SRJMET

Scientific Research Journal for Metal Engineering and Technologies ISSN:399-2017
Volume No.01 Issue No. 01, PP 106 - 119 01. Jan.2018

F- In sample I all parameters were constant, then friction time was changed and we obtained a good friction welding. Because the friction time was high and the friction pressure was still high.

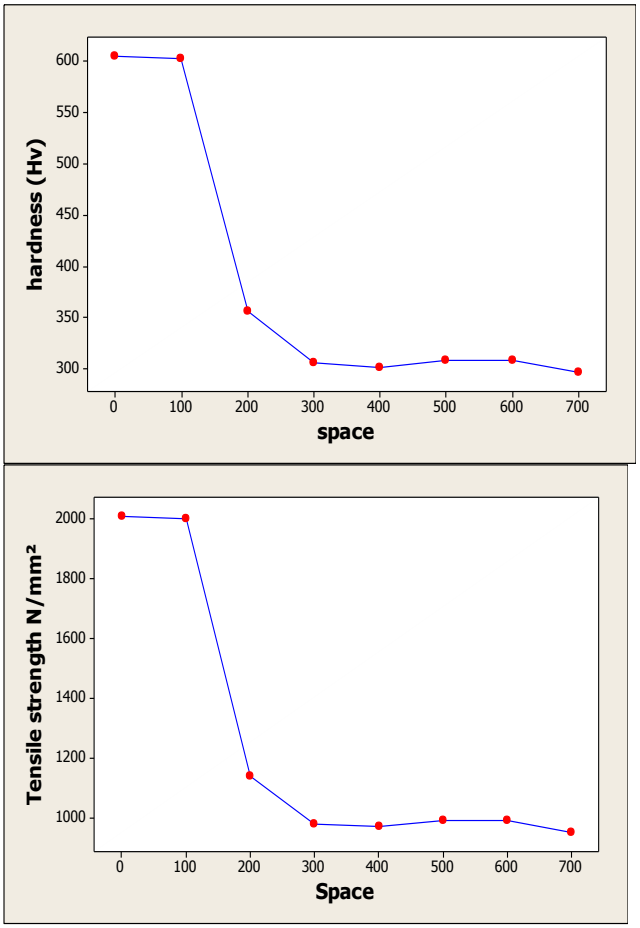

Figure 7 Hardness and tensile strength for Sample A. (After annealing)

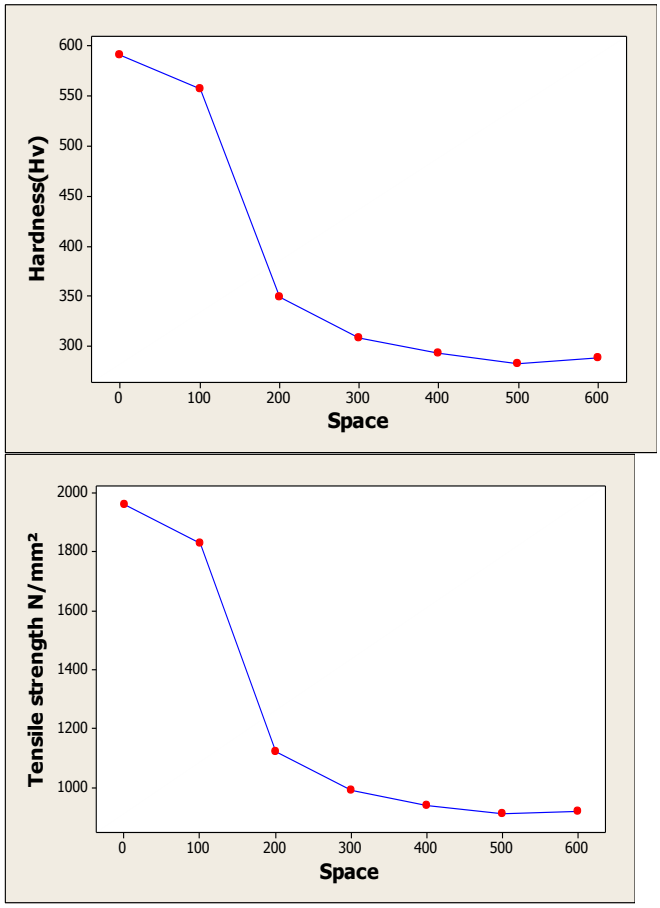

Figure 8 Hardness and tensile strength Sample B. (After annealing)

SRJMET

Scientific Research Journal for Metal Engineering and Technologies ISSN:399-2017
Volume No.01 Issue No. 01, PP 106 - 119 01. Jan.2018

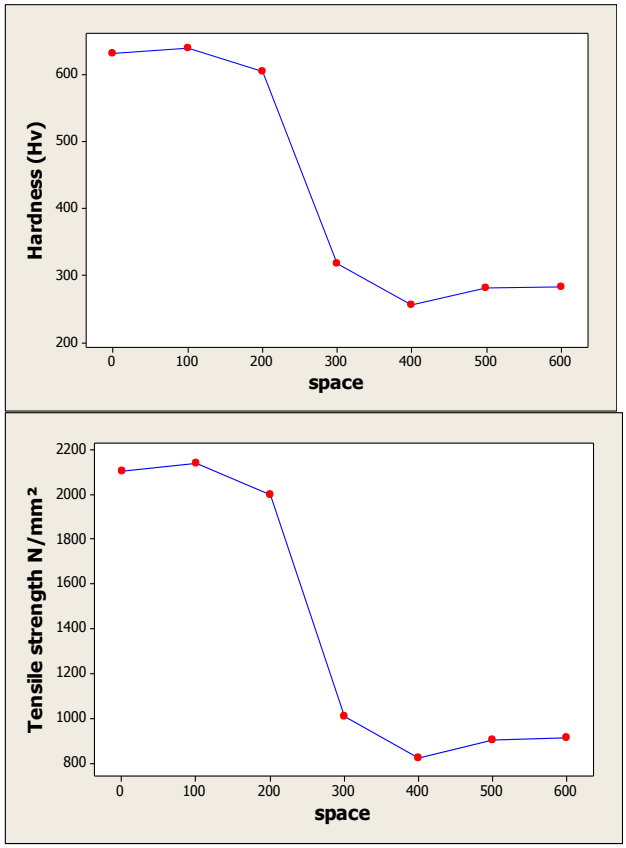

Figure 9 Hardness and tensile strength for Sample D. (After annealing)

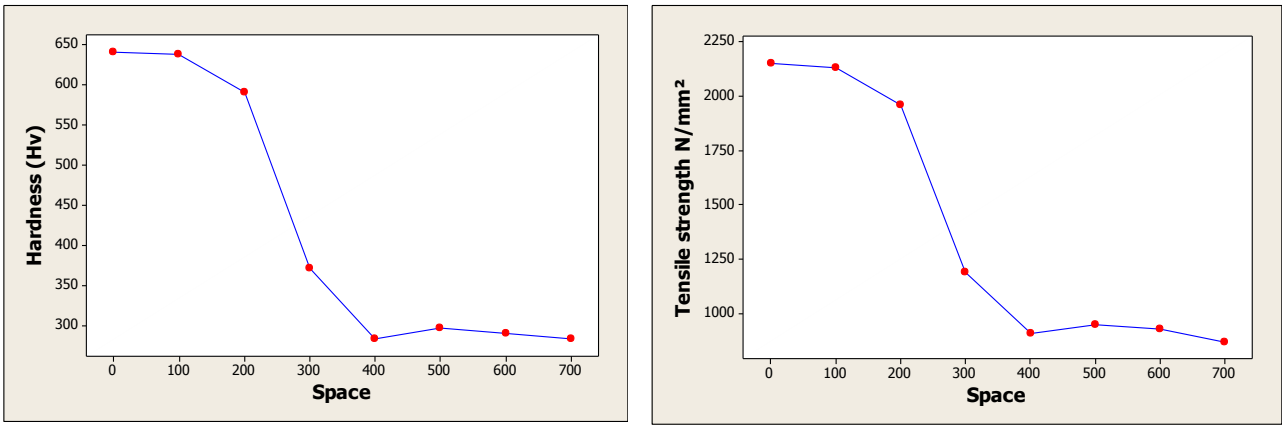

Figure 10 Hardness and tensile Sample I. (After annealing)

SRJMET

Scientific Research Journal for Metal Engineering and Technologies ISSN:399-2017
Volume No.01 Issue No. 01, PP 106 - 119 01. Jan.2018

4. The Optimum Investigated Parameters .

In this paper, the best friction welded joint obtained using parameters applied in sample 4 before annealing process. The Mechanical properties obtained using these parameters are the closest one to the original material properties as shown in Table 4m notably that the strength are measured according to the hardness.

Table 4 Hardness and Tensile strength of Base metal and Sample 4 (Before annealing)

Mechanical property	Hardness (Hv)	Tensile strength N/mm²
Base metal	390	1290
Sample 4	516.4	1690

Concerning the welding of annealed samples, the suitable friction welding parameters gives the best result refer to that used in the sample I. The mechanical properties obtained in this case exceed the original material properties as shown in Table 5.

Table 5 Hardness and Tensile strength of Base metal and Sample I (After annealing).

Mechanical property	Hardness (Hv)	Tensile strength N/mm²
Base metal	390	1290
Sample I	641.2	2150

5. Conclusion .

Friction welding of tool steel 1.2714 in different casers was investigated to arrange the suitable welding parameters. Some of the obtained experimental results give good welding joint with a high hardness and tensile strength compared to the base metal, this results marked in both conditions before and after annealing. The best tested friction welding parameters applied for the samples as received condition were Friction time 3sec forging pressure 70 bar, friction pressure 60 bar, rotation speed 1500 rpm. And After annealing for the base metal we get Optimum parameters of friction welding as Friction time 6sec forging pressure 70 bar, friction pressure 60 bar, rotation speed 1500 rpm

References .

1- Welding hand book, volume 2, welding processes, ninth Edition ,p.502-503.

2-Tool steels 5th Edition , George Roberts, George Krauss, Richard Kennedy,P1-6

3-Carbon Steel Handbook.(1014670), Final Report, March 2007.Dr. Kalamazoo, P.Flenner,p.10-19

4- Metals Hand Book Volume 6 welding brazing soldering .8th .P.25-30

SRJMET

Scientific Research Journal for Metal Engineering and Technologies
Volume No.01 Issue No. 01, PP 120 - 132

ISSN:399-2017
01. Jan.2018

ON THE VARIATION OF THE TENSILE PROPERTIES AND HARDNESS OF AISI 304 AUSTENETIC STAINLESS STEEL BY PLASTIC DEFORMATION

mabdulmula@yahoo.com

Abdulmula M. Mahaya[a] , **Mohamed M. Milad**[b]

a)Faculty of Engineering – Gharian

b)Faculty of Engineering – Tripoli

الملخـــــــــص :-

تتميـز عائلـة الصـلب الاسـتينيتي غيـر القابـل للصـداء وخصوصـا الصـنف AISI304 بمقاومـة عاليـة للصـداء فضـلا عـن سـهولة تشـكيلها وامتلاكهـا لخـواص ميكانيكيـة جيـدة الأمـر الـذي مكـن مـن اسـتخدامها علـى نطـاق واسـع فـي كثيـر مـن التطبيقـات الصناعية.

عنـد معالجـة هـذه السـبائك حراريـا لغـرض تلـدينها فأنـه يمكـن تشـكيلها بسـهولة للحصـول علـى قطـع صـناعية ذات أشـكال هندسـية معقـدة. غيـر أنـه ينشـأ عـن عمليـات التشـكيل المختلفـة المسـتخدمة فـي تصـنيع هـذه المـواد كالدرفلـة والثنـي والتجليـخ وغيرهـا مـا يعـرف بالتشـوه اللـدن والـذي ثبـت أن لـه تـأثير معتبـر فـي بنيـة الصـلب المستخدم وكذلك في خواصه الميكانيكية والمغناطيسية ومقاومته للصداء.

لـذا فـإن هـذه الورقـة تعـرض تـأثير التشـوه اللـدن النـاتج مـن عمليـة الدرفلـة علـى البـارد علـى خـواص الشـد وصـلادة الصـلب الاسـتينيتي غيـر القابـل للصـداء نـوع AISI304 .

عمليـا تـم تشـوه لـدن فـي صـفائح صـغيرة مـن الصـلب قيـد البحـث بدرفلتـه عنـد درجـة حـرارة الغرفـة بأعتبـار أن عمليـة الدرفلـة تسـتخدم علـى نطـاق واسـع فـي تشـكيل مثـل هـذه المـواد وقبـل تعـريض عينـات الصـلب المسـتلم الـى عمليـة درفلـة فأنـه تـم معالجتهـا حراريـا بتسـخينها حتـى درجـة الحـرارة 1050 م لمـدة سـاعة قبـل ان يـتم غمرهـا بالمـاء. ومـن تـم أمكـن الحصـول علـى ثـلاث نسـب درفلـة مختلفـة وهـي 20%، 40% و 60%.

أظهـرت نتـائج هـذه الدراسـة زيـادة واضـحة فـي مقاومـة الخضـوع ومقاومـة الشـد القصـوى الصـلادة بزيـادة نسـبة الدرفلـة وبـوثيرة متشـابهة بينمـا نقصـت المطيليـة إلـى

SRJMET

Scientific Research Journal for Metal Engineering and Technologies
Volume No.01 Issue No. 01, PP 120 - 132

ISSN:399-2017
01. Jan.2018

قيمة متدنية جدا بما يفسر أستجابة هذا النوع من الصلب الى ظاهرة التقوية بفعل عملية الدرفلة على البارد.

أوضحت النتائج أيضا أن أعلى نسبة زيادة فى مقاومتي الخضوع والشد وكذلك الصلادة حصلت عند نسبة الدرفلة 20% ومن تم لوحظ زيادة بسيطة في كليهما عند نسبتي الدرفلة40% و 60%.

ABSTRACT.

Austenatic stainless steels, in particular type AISI304 stainless steel are interesting engineering materials used for structural purposes as they offer a wide range of corrosion resistance, apart from excellent fabrication and mechanical properties.

A fully annealed austenitic stainless steel can be formed to complex shapes easily. However, during fabrication this steels are subjected to various forming processes including rolling, bending, ……..etc. Hence, these steel alloys usually suffer from severe plastic deformation that has a substantial influence on their structure, mechanical and magnetic properties as well as corrosion resistance.

Accordingly, this paper addresses the influence of plastic deformation on the tensile properties and hardness of AISI304 austenitic stainless steel.

Small strips of AISI304 SS are deformed at room temperature by cold rolling as it is widely used in fabrication processes of such materials. Before rolling the strips were solution annealing at 1050C for one hour. Three different percentages of cold reduction mainly 20%, 40% and 60% were obtained by the same manner. The results indicate that the yield strength, the ultimate tensile strength and the hardness were found to be increased with increasing the cold rolling reduction almost by the same tendency whereas the ductility is extensively reduced to a very small value. This behavior indicates the response of the tested steel to the strengthening phenomenon as a result of cold rolling. Furthermore, it was shown that the highest percentages increase in the strength and hardness of AISI304 SS

occurred at 20% cold reduction. Thenaftera little increase in such properties was noticed at 40% and 60% cold work

Key words: Stainless steels, work hardening, tensile properties, martensitic transformation

1. INTRODUCTION.

Austenitic stainless steels (ASS) are the most common and familiar types of stainless steels. They can be made soft enough to be easily formed by annealing. However they cannot be hardened by quenching to room temperature like other metals. Rather cold working is considered to be a convenient strengthening method of such steels since they normally have a high strain hardening coefficient. Cold forming is indispensable processes that is widely used for austenitic stainless steels and there is growing interest in the effect of prior cold work on the properties of this kind of materials.

During the processing or service, cold worked ASS may present complex microstructural changes such as stacking faults, stacks faults bundles or faulted ε- martensite, deformation twins, deformation bands and ά martensite besides intensive dislocations multiplications [1].

Perhaps the most common aspect of cold worked ASS is the formation of strain-induced martensite that may be considered as a unique factor of such materials when cold rolled.

ASISI 304 SS becomes microstructurally unstable at room temperature when deformed and transformed to ά martensite. Therefore the appearance of martensite changes the single phase state of such steel in a way that their mechanical and magnetic properties are altered.

The ά martensite transformation increases the work hardening rate during deformation and this effect is known to be beneficial to formability of AISI 304 SS. The additional strengthening obtained with ά martensite phase may also be used in practice to save weight. In this aspect, martensite formation resulting from plastic deformation of metastable austenite is of a great interest for producing high strength and ductility.

For severe cold forming operations such as the cold hardening of bolts very low work hardening rates are required. In contrast the cold forming of stainless steel strip may require material which can undergo severe stretching. In this case relatively high rates of work hardening are required. A good example is the production of stainless steel sinks which undergo severe deformation in achieving their final shape without the need for the inter-stage annealing.

Different studies on the effect of cold deformation on austenitic stainless steels have been made to correlate the mechanical and magnetic properties of AISI 304 SS to the degree of deformation[2], to analyze the cold rolling texture in AISI 304SS [3], to evaluate the phase transformation induced by severe plastic deformation in the AISI LSS[4], to study the effect of cold working on pitting corrosion[5] and sensitization of ASS [6].

As cold rolling is vital processes in forming 304SS, the aim of this work is to test the effectiveness of such processes in producing a 304 SS combining high strength, hardness and ductility to further rise its strength during technological forming.

Meanwhile as cold work is known to have a substantial influence on the corrosion behavior of deformed ASS , there should be a compatible between the strength and the corrosion resistance of the selected steel used in the application wherein a high corrosion resistance is required besides adequate strength as being recommended in some standards.

2. EXPERIMENTAL WORK

2.1 MATERIAL

The material used in this study was a commercial grade type 304 stainless steel used in sheet form of three millimeters thickness.

The nominal chemical composition of the AISI 304SS used in this work obtained by an emission spectroscopy is shown in table (1).

Table 1: Nominal chemical composition of 304 stainless steels

Element	C	Cr	Ni	Mo	Mn	Cu	Si	Fe
Composition Wt %	0.04	17.21	7.5	0.23	1.58	0.31	0.66	Balance

The original steel sheet of 300x300x3 mm was sectioned into small strips of 200x60 x3 mm being suitable for cold rolling process.

2.2 SOLUTION ANNEALING HEAT TREATMENT

The solution annealing heat treatment was carried out in a Nabertherm furnace of 1200°C maximum working temperature. It was carried out in order to achieve chemical homogeneity and to dissolve any carbides that might be present in the as received steel samples.

The solution annealing heat treatment was done at 1050°C for about one hour soaking time and then the samples were quenched in water of approximately room temperature.

All steel strips were stirred heavily in the liquid bath to obtain maximum cooling rate. The solution annealed specimens will be referred as (SA).

2.3 COLD ROLLING .

The rolling process was used in this work in order to have a uniform thickness and flat shape. The cold rolling has been done for the annealed strips at room temperature using a two - high mill rolling machine.

Rolling process was carried out under oil lubrication to prevent over heating of steel strips which may affect the structure of the steel. To avoid modulation, the steel strips were cold reduced by many successive passes in one direction and gradually reduced their thickness to the required percentage. The total number of passes required to obtain the desired cold reduction was found to increase with increasing the percentage of thickness reduction.

Three different percentages of cold reduction (%CR) were obtained (20%, 40% and 60%). The %CR was calculated with respect to the thickness reduction using this formula:

$$\%CR = \frac{t_0 - t_f}{t_o} x100 \quad \ldots\ldots(1)$$

Where:

t_o = the thickness of the specimen before rolling

t_f = the thickness of the specimen after rolling.

2.4 HARDNESS TEST

The macro- hardness measurements was carried out on samples of as received, solution annealed and cold worked strips (20%, 40% and 60%) at similar positions along the length of each strip using Rockwell hardness tester, in a way that the solution annealed and as received strips was tested with (B) scale as they have lower hardness values. The cold rolling specimens were measured using scale (C) as they exhibit higher values of hardness.

All recorded values are the average of eight readings. For comparison, all hardness values were converted into Vickers hardness using hardness conversion tables.

2.5 TENSILE TEST.

Tensile test was performed on solution annealed and cold worked samples using a 500 KN universal testing machine at constant cross beam travel of 0.5 mm/ min. A minimum of three samples were tested for each condition and the average was taken. The yield strength, the ultimate tensile strength and percentage of elongation to failure were recorded for each sample.

2.6 METALLUGRAPHIC INSPECTION.

Small specimens were sectioned for each stripe, as received, solution annealed and various cold rolled samples for the metallurgical inspection.

The specimens were mounted, ground, polished, etched in (10% HCL, 30% NH_3 and 60% H_2O) and viewed by using optical microscope at various magnifications.

SRJMET

Scientific Research Journal for Metal Engineering and Technologies
Volume No.01 Issue No. 01, PP 120 - 132

ISSN:399-2017
01. Jan.2018

3. RESULTS AND DISCUSSION.

3.1 EFFECT OF COLD ROLLING ON HARDNESS

The influence of some cold working percentages is presented in table (1). Figure (1) shows that a cold reduction of 304 SS by 20% has caused a substantial increase in its hardness. The percentage increase is about 130%. This result may be related to the lower hardness of the solution annealed samples compared to that of as received once which has a hardness of 190HV. The microstructure of the solution annealed sample reveals irregular coarse ductile austenite grains compared to that of as received one Figure (3a). Furthermore, the elimination of grain boundary carbides from the as received steel Figure 3.3b by the solution annealing heat treatment may have contribution in reducing the hardness of the solution annealed steel. As 304 SS is further rolled beyond 20% CR, a little increase in the hardness is noticed in Figure 1. Increasing %CR from 20% to 60% has raised the Vickers hardness by only 15%. That is to say that as 304SS is plastically deformed, its hardness seems to become less sensitive to cold working.

Table 2: Hardness test results

Sample No.	SA	20%CR	40%CR	60%CR
Average, HV	160	380	420	440

Note:As received hardness = 190HV

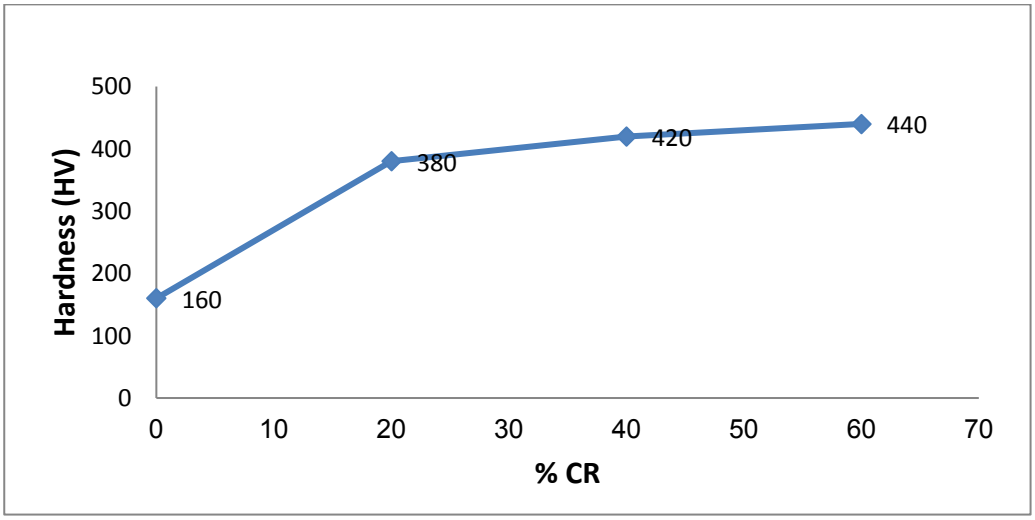

Figure (1):Effect of cold rolling on Vickers hardness

3.2 EFFECT OF COLD WORK ON TENSILE PROPERTIES .

The tensile properties of various cold rolled 304SS samples are predicted in table 3 and shown in Figure(2). The yield strength, tensile strength and ductility are shown to be extremely affected by the first step of cold reduction (20%CR). In this aspect more than 50% and130% of percentage increase in tensile strength and yield strength respectively are noticed. Nevertheless, like the hardness as the %CR is increased both tensile strength and yield strength seem to be less relevant to cold work.

It is to be noted that the variation between yield strength and tensile strength becomes so small at 40%Cr and 60%CR. In another way, the gap between the two curves of yield strength and tensile strength of Figure (2) becomes narrower. Accordingly it may be expected by extrapolation that at higher values of (above 60%CR), 304SS may behave like a brittle material, the above observation cab be assisted by the ductility curve of Figure (2) which shows a sudden decrease in the percentage of elongation (EL%) at 20%CR. Meanwhile at 40%CR and 60%CR the effect of CR% on EL% becomes negligible which indicates that the tested 304SS has undergone a strengthening process with almost zero ductility.

Table (3): Tensile test results

Sample No.	UTS (N/mm2)	Y.S (N/mm2)	EL%
SA	727	425	37%
20%	1110	985	16%
40%	1259	1204	6%
60%	1342	1302	4%

Knowing that austenite stainless steel cannot be hardened by heat treatment and can be only hardened by cold working, the enhancement of strength and hardness of 304SS may be attributed mainly to the strain or work hardening that is

characterized ASS. In this aspect ASS are one of the most metals that are highly respond to strain hardening phenomenon. The value of the strain hardening exponent (n) of some ASS is reported to be 0.52 which almost equals to that of copper (0.54) and being about three times that of annealed carbon steel (0.15). [7].

Accordingly, the dislocation density though to be highly increased during low levels of cold reduction whereas at high levels of cold work, ASS may get saturation of dislocation in a way that the strength and hardness of ASS don't increase with increasing %CR. It is to be emphasized that martensitic transformation is a unique feature of ASS when they are cold worked. Martensite is shown to be formed more likely in the interior of deformed austenite grains Figure 3.3c,d. However, the change in the tensile properties and the hardness was found to be irrelevant to martensite formation in the tested steel, rather the strain hardening is considered to be much more important. In this regard, the increase in the martensite content with increasing %CR as anticipated by the microstructure of cold worked strips Figure 3.3 is not accompanied by the corresponding increase in the strength and hardness of the tested 304SS. Moreover, the sharp change in the tensile properties and the hardness occurred at 20%CR could not be well attributed to the slight increase in the strain-induced martensite formed at such low %CR as being reported by many researchers, see for example [3,8]

On contrary, more martensite is reported to form at higher amounts of plastic deformation [9], but such high contents of martensite phase don't result in an equivalent increase in the yield and tensile strengths as well as hardness Figures (1,2) as it is expected to do. Therefore, one may exclude the role of strain-induced martensite in strengthening the investigated 304SS in this study.

SRJMET
Scientific Research Journal for Metal Engineering and Technologies
Volume No.01 Issue No. 01, PP 120 - 132
ISSN:399-2017
01. Jan.2018

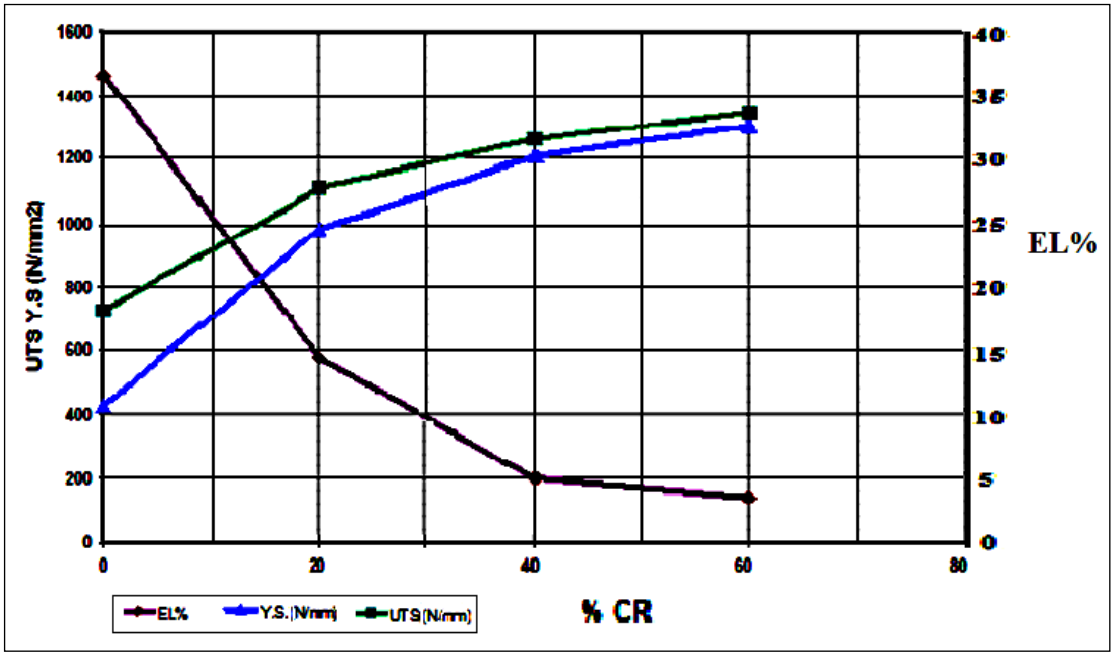

Figure (2): Effect of cold rolling on tensile properties

3.3 EFFECT OF COLD WORK IN MICROSTRUCTURE.

Figure 3 shows the microstructures of as received, solution annealed, and various cold rolled 304SS specimens.

The microstructure of as received steel Figure(3.a) represents typical microstructure of 304SS that consists of small austenite grains of normal shapes. Solution annealing heat treatment alters the morphology of the austenite grains in such that the grains being of a semicircular shape and their sizes get enlarged (coarsening) Figure (3d) that may be as a result of a relatively prolonging soaking time as compared to the small thickness of the received steel sheet.

Cold working of 304SS as shown in Figure (3c-e) has introduced the following features:

1 - The austenite grains are heavily deformed in the direction of rolling, in particular after 60%CR.

2 – Fine grains are shrinked and the coarse grains are grown feathers i.e, the large grains are coarsened on the expense of the small one.

Scientific Research Journal for Metal Engineering and Technologies
Volume No.01 Issue No. 01, PP 120 - 132
ISSN:399-2017
01. Jan.2018

3 – The grain boundary area is progressively reduced.

4 – The formation of strain-induced martensite (very fine parallel lines) prudentially I the interior of the austenite grains as well as within the slip bands.

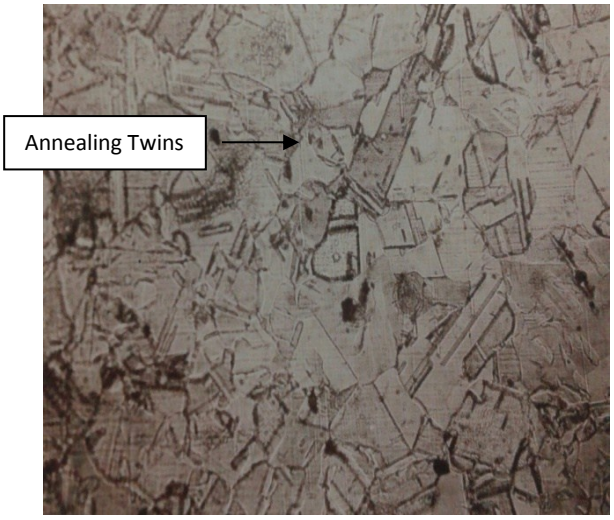

a

b

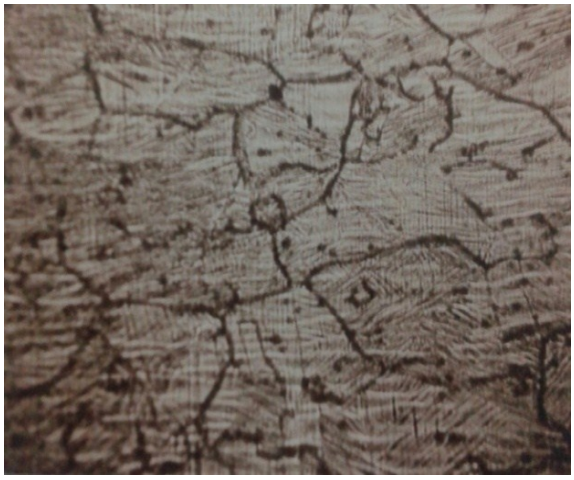

c

d

SRJMET
Scientific Research Journal for Metal Engineering and Technologies
Volume No.01 Issue No. 01, PP 120 - 132
ISSN:399-2017
01. Jan.2018

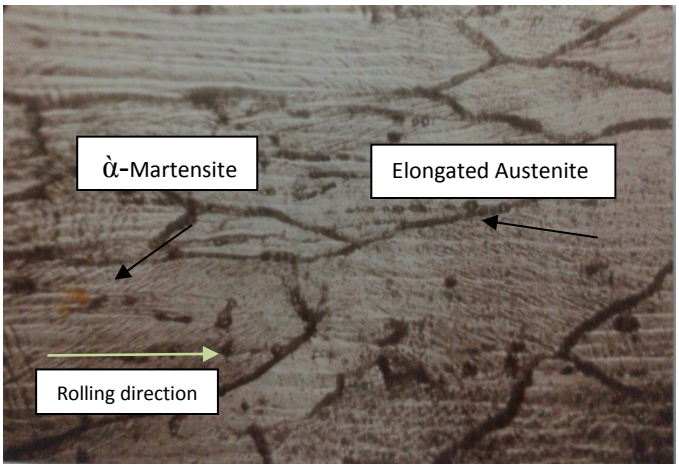

e

Figure (3): Microstructures of 304SS samples. (a) as received, (b) solution annealed, (c) 20%CR, (d) 40%CR and (e) 60%CR . (400x)

CONCLUSIONS.

The following conclusions can be withdrawn from the present work:

1-Type AISI 304 austenetic stainless steel displays a considerable strengthening as a result of cold rolling.

2- The yield strength, tensile strength and hardness of 304SS are found to be substantially increased at 20%CR. However the influence of 40% and 60%CR is observed to be less pronounced.

3- Strain-induced martensite is shown to be formed more likely at the interior of austenite grains. Meanwhile its role in strengthening the tested 304SS is not realized unless its volume fraction (at least) is identified.

REFERENCES.

1-Padilha. A.F, Plaut.R.L, Rios. P.R, ISIJ International, 43,2003,P. 135.

2- Kurc. A, Stoclos. Z, AMSE J, 34, 2008, P.89.

3- Ravi Kumar. B, Singh. A.K, Samar Das, Bhattacharya. D. K, J. Mat. Sci. and Eng.,

A 364, 2004, P. 132.

4- Tavares. S.S.M, Gunderov. D, Stolyarov. V, Neto. J.M, J. Mat. Sci. and Eng., A 358,

2003, P.32.

5- Peguet. L, Malki. B, Baroux. B, J. Corr. Sci., 51, 2004, P. 493.

6- Raghuvir Singh, Ravkumar. B, Kumar. A, dey. P.K, Cattoraj. I, J. Metall. And Mat.

Trans., 34A, 2003, P. 2443.

7-Low J. R. "Properties of Metls in Materials Engineering" American Society For

Metals, Metals Park, Ohio, 1949.

8- Kain,V, Chandra K, Adhe,K. N, P. K. De, J. Nucle. Mat, 334, 2004, P. 115.

9- Peguet L, Malki B, Baroux B, J. Corr. Sci, 49, 2007, P. 1933.